A COUPLED ANALYSIS OF THERMAL AND ELECTROMAGNETIC PHENOMENA DURING HYPERTHERMIA IN BIOLOGICAL TISSUES

A Thesis Submitted
In Partial Fulfilment of the Requirements
for the Degree of

MASTER OF TECHNOLOGY

by

SNEHANSU MANDAL

to the

DEPARTMENT OF MECHANICAL ENGINEERING
INDIAN INSTITUTE OF TECHNOLOGY, KANPUR

JULY, 1988

CERTIFICATE

This is to certify that the thesis entitled, "A Coupled Analysis of Thermal and Electromagnetic Phenomena during Hyperthermia in Biological Tissues" by S. MANDAL, is a bonafide record of work done by him under our guidance and supervision, for the award of the Degree of Master of Technology at the Indian Institute of Technology, Kanpur, The work carried out in this thesis has not been submitted elsewhere for the award of a degree.

(Dr. T. Sundararajan)
Assistant Professor
Department of Mechanical Engineering, IIT Kanpur

(Dr.P.S.Ghoshdastidar)
Assistant Professor
Department of Mechanical Engineer
Indian Institute of Technology
Kanpur

July, 1988.

ACKNOWLEDGEMENTS

I express my deep sense of gratitude to Dr.T.Sundararajan and Dr. P.S. Ghoshdastidar for suggesting the problem and sorting out various difficulties throughout the course of this thesis. I also thank them for their contributions, made by way of timely advice and criticism.

July, 1988

-S. Mandal

CONTENTS

LIST OF TABLES

LIST OF FIGURES

NOMENCLATURE

B	Non-dimensional decay constant defined by equation (2.28b)
C	Speed of electromagnetic wave propagation in a medium
C_p	Specific heat
$\underline{E}$	Electric field intensity vector
$\underline{H}$	Magnetic field intensity vector
h	Convective heat-transfer coefficient
K	Extinction co-efficient defined by equation (2.11)
K_t	Thermal conductivity of tissue
L	Length of the solution domain in x-direction
N_i	Shape functions for the 8-noded isoparametric element
Bi	Biot number
n	Refractive index defined by equation (2.10)
Q	Energy absorption rate per unit volume of tissue defined by equation (2.24)
q	Heat-transfer coefficient
r_e	Electrical resistivity of tissue
S	Instantaneous rate of energy transport per unit area through tissue medium (Poynting vector) defined by equation (2.13)
T	Temperature of tissue medium
t	Time
W	Perfusion rate

X,Y,Z	Three perpendicular coordinates.

GREEK LETTERS:

ω	Frequency of electromagnetic radiation
γ	Electrical permittivity of tissue
μ	Magnetic permeability of tissue
λ	Wavelength of EM radiation in tissue
ρ	Density
ξ,η	Local coordinates
θ	Fraction of implicit differencing for time discretization.

SUBSCRIPTS:

a	artery
amb	ambient
b	blood
f	fluid (air)
o	air or vacuum
r	relative
t	tissue
X	in X-direction
Y	in Y-direction
Z	in Z-direction
Y,O	along Y-direction in air or vacuum
Z,O	along Z-direction in air or vacuum
YM	Maximum value in Y-direction
ZM	Maximum value in Z-direction

SUPERSCRIPTS:

*	Non-dimensional.

ABSTRACT

A finite element analysis of hyperthermia in biological tissues has been performed. The coupled thermal and electromagnetic phenomena have been studied in detail. The bio-heat transfer equation has been used for thermal modelling. Two separate cases have been analysed, one with a fixed rate of blood perfusion through the tissue and the other with blood perfusion varying as a function of tissue average temperature and time. A two-dimensional problem with rectangular geometry has been considered for the sake of simplicity, although the formulation can be easily extended to 3-D or more complex geometries. The electromagnetic radiation is taken to be coherent and two plane polarized.

The governing equation has been solved by the finite element method using 8-noded isoparametric elements. Transient temperature results within the tissue have been obtained using the Frontal algorithm for matrix solution and marching in time using implicit finite differencing. Results have been presented for steady state temperature profiles, transient temperature variation at tissue centre and isotherm patterns, for various hyperthermia conditions. The effects of varying Specific Absorption Rate (SAR), rate of blood perfusion and the frequency of radiation, have been highlighted for two types of tissues, namely, the human

thigh muscle and the human lung.

The numerical results have been validated by comparing with an analytical solution for the steady state problem with two adiabatic boundaries. The results indicate that the temperature increases with SAR linearly and decreases with blood perfusion non-linearly. However, the temperature rise is less sensitive to changes in rate of blood perfusion. For the case of automatically changing blood perfusion rate, the tissue temperature displays an overshoot above the final steady state value. At low radiation frequency, the rate of heating is more and it penetrates deeper. As for the electromagnetic properties of the tissues, the dielectric constant plays an important role in determining the level of temperature rise.

CHAPTER 1

INTRODUCTION

1.1 GENERAL BACKGROUND:

Now-a-days cancer treatment is attracting more and more attention from medical personnels and technologists all over the world, as cancer is still one of the deadliest diseases which has defied man. Hyperthermia by high intensity microwave heating is one of the most effective methods that are being applied for cancer-treatment. The present work attempts to develop a detailed theoretical model for micro-wave heating of biological tissues, taking into account the electro-magnetic interaction between the tissues and the micro-wave radiation.

It is well known that there is a critical temperature for biological cells (around $43^{\circ}C$ - $45^{\circ}C$), beyond which the cell dies. This limiting temperature is called the tumoricidal temperature. If a certain portion of the human body containing the cancerous tissue is treated beyond the tumoricidal temperature, while the surrounding tissue is below this critical temperature, the cancerous cells can be destroyed selectively without affecting the other cells of the body.

1.2 DESCRIPTION OF HYPERTHERMIA:

In this process, the portion of the body, to be heated locally, is exposed to a high frequency electro-magnetic radiation. The frequency of the radiation may be in the short-wave radio-range or in the micro-wave range. Short-wave diathermy has been assigned the frequencies of 13.5, 27.12and 40.68 MHz, while the micro-wave diathermy has been assigned the frequencies of 915, 2450, 5850 and 18000 MHz. 'Short-wave' diathermy provides deeper and more uniform heating than the diathermy at higher frequencies. Here we shall briefly discuss the inter-action between the electromagnetic radiation and the biological materials during hyperthermia.

When the electro-magnetic wave passes through a certain medium, both electric and magnetic fields, which are perpendicular to each other and also to the direction of propagation of the wave, are produced. The interaction of these two fields gives rise to electromagnetic energy, which is carried by the travelling wave. When the wave passes through vacuum or air, the energy associated with it remains unattenuated with distance. But when the electromagnetic radiation passes through a dielectric medium of finite-electrical resistivity (such as the biological tissue), the energy of the EM radiation is attenuated gradually along the direction of propagation of the wave. This is due to the fact that the energy

of the wave is absorbed within the tissue at each point along the path of the wave. The electromagnetic energy absorbed by the tissue manifests itself in the form of heat, which raises the temperature of the tissue. The rate of heat absorption depends on the nature of the dielectric medium and also on the nature of the electromagnetic radiation being incident. The rate of energy absorption increases for medium with higher values of dielectric constant.

1.3 DISCUSSION OF AVAILABLE LITERATURE:

Several electrical, medical and heat-transfer scientists have contributed to research on the analysis and technology of hyperthermia.

Baish, Foster and Ayyaswamy [1] developed a parametric study for the relationship among the tube size, tube spacing, material properties and the simulated perfusion rate using perfused phantom models of microwave irradiated tissues. They used a parallel tube heat exchanger configuration to simulate the internal convection effects of blood flow. The measured thermal response of the phantom was seen to be favourably comparable with the numerical solution of the bio-heat transfer equation under the same irradiation conditions. Thus they provided experimental evidence for the successful use of the bio-heat equation for modelling the thermal response of real tissues.

The same authors [2] developed analytical expressions for the local temperature fluctuation near isolated and counter-current blood vessels during hyperthermia. These scaling laws relate the magnitude of such fluctuations to the size of the heated region and to the thermal equilibration length of the vessels. They have shown that counter-current vessels have shorter equilibration length and produce smaller temperature fluctuations than isolated vessels of the same size. Baish et al. [3] also conducted a parametric comparison of three different vascular models, namely, (i) an array of unidirectional vessels, (ii) an array of counter-current vessels and (iii) a set of large vessels feeding small vessels which then drain into large vessels for describing heat-transport in tissue. Analytical and numerical methods were used to predict the gross temperature distribution throughout the tissue and the small scale temperature gradients associated with thermally significant blood vessels. They have shown that three continuum formulations of bio-heat transfer (directed perfusion, effective conductivity, and a temperature dependent heat-sink) are limiting cases of the vascular models with respect to the thermal equilibration length of the vessels.

Weinbaum, Jiji and Lemons [4] used the tissue clearance method for preparing vascular casts of the rabbit thigh and sectioned them parallel to the skin surface to determine the detailed variation of the vascular geometry

as a function of tissue depth and proposed a new three layer model for the deep tissue, skeletal muscle and cutaneous layers. In a latter work [5], they developed the above model into a detailed quantitative model which takes into consideration the variation of the number density, size and flow velocity of the counter-current arterio-venous vessels as a function of the depth from the skin surface, the directionality of blood perfusion in the transverse vessel layer and the superficial shunting of blood to the cutaneous layer.

Weinbaum and Jiji [6] also developed a simplified 3-D bio-heat equation to describe the effect of blood flow on blood-tissue heat-transfer. They derived a simple expression for the tensor conductivity of the tissue as a function of the local vascular geometry and the flow velocity in the thermally significant counter-current vessels. They have also shown that directed (as opposed to isotropic) blood-perfusion between the counter-current vessels can have a significant influence on heat-transfer in regions where the counter-current vessels are under 70- μm diameter.

Arkin, Holmes, Chen [7] have performed a sensitivity analysis using a theoretical model of pulse decay method for the determination of local tissue thermal conductivity and blood perfusion rate. It is based on a comparison of

the measured temperatures with the theoretically calculated temperatures. They have shown that a chosen pulse duration of 3 seconds is in agreement with the analysis as a good compromise between accuracy and excessive tissue heating. The same authors have described in a later paper [8], the theoretical model upon which the TPD method is based and have detailed its capabilities and limitations.

Valvano, Allen and Bowman [9] have presented an improved technique for the determination of the thermal conductivity, the thermal diffusivity, and the blood perfusion using a self-heated spherical thermistor probe. In this paper, it has been shown that in the presence of flow, the transient power response does not follow $t^{-1/2}$ as has been previously assumed. Here, firstly, effective thermal properties are measured and then perfusion is quantified from effective thermal properties.

Sekins, Emery, Lehmann and MacDougall [10] have shed light on the blood flow response occurring during local hyperthermia in muscle through a two-dimensional transient thermal model of human thighs undergoing microwave diathermy. The model blood flow values were checked against those measured in the human subjects via xenon 133 wash out method and good agreement was found.

Foster et al. [11] have examined the heat-transfer characteristics of biological bodies which are subjected to strong microwave fields with simultaneous

cooling by flowing water to estimate the maximum temperature increase and the thermal tissue constants that are encountered during typical hyperthermia experiments.

Diller and Hayes [12] have modelled the burn process resulting from the application of a hot, cylindrical source at the skin surface using the finite element technique. Here a rotationally symmetric 125 element mesh was defined within the tissue beneath and outside of an applied heating disk. Natural convection with ambient air was assumed for areas of skin surface not in direct contact with the disk.

Newman and Lele [13] have proposed several techniques to measure the local thermal diffusion in tissue by heating with a focussed ultrasound field. Transient as well as near steady state heat inputs have been considered and examined for their suitability of being the measurement techniques for either tissue thermal diffusivity or perfusion rate.

Elkowitz, Shitzer and Eberhart [14] have numerically solved the bio-heat transfer equation to calculate the temperature profiles in tissues subjected to non-uniform blood flow distribution for initial and boundary conditions which simulate experimental physiological situations. The methods and results are useful for the prediction of temperature profiles in the absence of significant endogenous or exogenous heating.

J.F. Deford and O.P.Gandhi [15]have used the impedance method for solving low frequency dosimetry problems in three-dimensional geometries involving lossy dielectrics. The scattering object has been modelled with an equivalent impedence network. Their results indicate that the contact electrodes produce relatively uniform deposition between the plates in the region of torso, whereas the loop applicator studied gives rather large deposition near the surface of the body, especially in the spinal region, and very small deposition in the core of the body.

J. Behari [16] has dealt with the phenomenon of dielectric dispersion and mechanism of microwave interaction in biological media. He has also cited several electrical methods for measuring the electrical properties of tissue.

O.P. Gandhi, J.Y. Chen and A. Riazi [17] investigated how currents are induced in a human being subjected to microwave radiation. They have also discussed about the safety guidelines regarding the induced current.

Thus the available literature indicates that the research studies have so far concentrated selectively on the physiological or thermal or electrical aspects of hyperthermia in biological materials. More research is required to be performed on the coupled nature of the various processes during hyperthermia.

1.4 SCOPE AND OBJECTIVES OF THE PRESENT STUDY:

The present study deals with a coupled thermal and electromagnetic model of hyperthermia in biological tissues by microwave radiation. For the sake of simplicity, a two dimensional rectangular geometry has been considered. However, the problem formulation is of a very general nature and it can easily be extended to axi-symmetric and three-dimensional problems. The applied electromagnetic radiation is assumed to be polarised such that the wave propagates only in x-direction.

The objectives of the present work are to predict the temperature distribution within a tissue of the human-body and ascertain the portions which will be destroyed by radiation. The following specific aspects of the problem will be considered:

i) To predict the range of power of the micro-wave radiation that can be used to destroy the cancerous tissue selectively.

ii) To show the effects of different radiation frequencies upon the temperature profile at the same power input and blood perfusion rate for a given tissue.

iii) To demonstrate the effects of constant and time dependent blood perfusion rates upon

the heat-transfer characteristics of the hyperthermia process. For the time dependent case, the blood perfusion rate will be assumed to depend upon the average tissue temperature and also explicitly upon time.

iv) To highlight the influence of the electromagnetic properties of the tissue by performing the analysis for different tissue materials.

CHAPTER 2

THERMAL MODELLING

2.1 INTRODUCTION:

In the earlier days, the detailed processes which occur during the passage of microwave radiation through biological tissues were not well understood. It was believed that the destruction of tissues by microwave radiation was due to electrical phenomena. Later it became established that thermal effects chiefly contribute to the cell destruction during hyperthermia. In the present study of hyperthermia by microwave radiation, the electro-magnetic interactions are taken into account through Maxwell's field equations and the thermal processes are modelled via the bio-heat equation.

Many studies have so far been performed on heat-transfer analysis in biological tissues using the bio-heat equation. But none of them have so far used the Maxwell's field equations to predict the rate of heat generation for unit volume of tissue. In these analyses, a uniform heat source of given intensity has been assumed. In the present study, an attempt has been made to predict the rate of heat generation at any given location using only the electro-magnetic properties of the tissue material and the characteristics of the microwave radiation. Thus actual

problem parameters such as the intensity of radiation and the microwave frequency are directly involved in the analysis. Also the specific nature of the tissue being subjected to hyperthermia is taken into account through the use of appropriate thermal properties (i.e. density, specific heat and thermal conductivity) and the electro-magnetic properties such as the electrical resistivity, electrical permittivity and magnetic permeability.

Another important parameter in bio-heat equation, which controls the rate of tissue heat-up, is the local blood perfusion rate. The proper evaluation of this parameter is complicated by the fact that the physical and mental response of the human body to any stimulus, say, that of the micro-wave heating, is very complex. It has been observed that the blood perfusion rate is different at different locations of the human body. It also varies with time, temperature of the tissue, physical and mental conditions of the subject and so many other environmental factors. An accurate correlation of blood perfusion rate with its influencing factors is yet to be established. Keeping all these facts in mind the present study is restricted to two specific situations of blood perfusion.

i) In the first case, the blood perfusion rate has been considered to be constant with time and tissue temperature.

ii) In the second case, blood perfusion rate has been considered to vary with time and the average temperature of the tissue. An experimental correlation from [10] has been used to calculate the blood perfusion rate.

2.2 MATHEMATICAL MODELLING:

The transient heating of a rectangular tissue with microwave radiation has been considered. A two-dimensional [Fig.2.1 situation has been modelled here for the sake of simplicity although the formulation can be very easily extended to 3-D or axisymmetric geometries. The electromagnetic radiation is taken to be corresponding to that of a polarized unidirectional wave. The rate of blood perfusion is assumed to be uniform throughout the tissue. The initial temperature of the tissue at time t = 0 (just at the start of heating) is taken to be equal to the normal body temperature of $36^{\circ}C$. The outside atmospheric temperature is assumed to be $27^{\circ}C$. The thermal and electromagnetic properties [Table 2.1] of the tissue are taken to be uniform spatially and constant with respect to time. With these assumptions, the temperature-time response of the tissue has been estimated using the bio-heat equation.

2.2a BIO-HEAT EQUATION:

The energy conservation principle applied to the biological tissue undergoing diathermic or microwave heating,

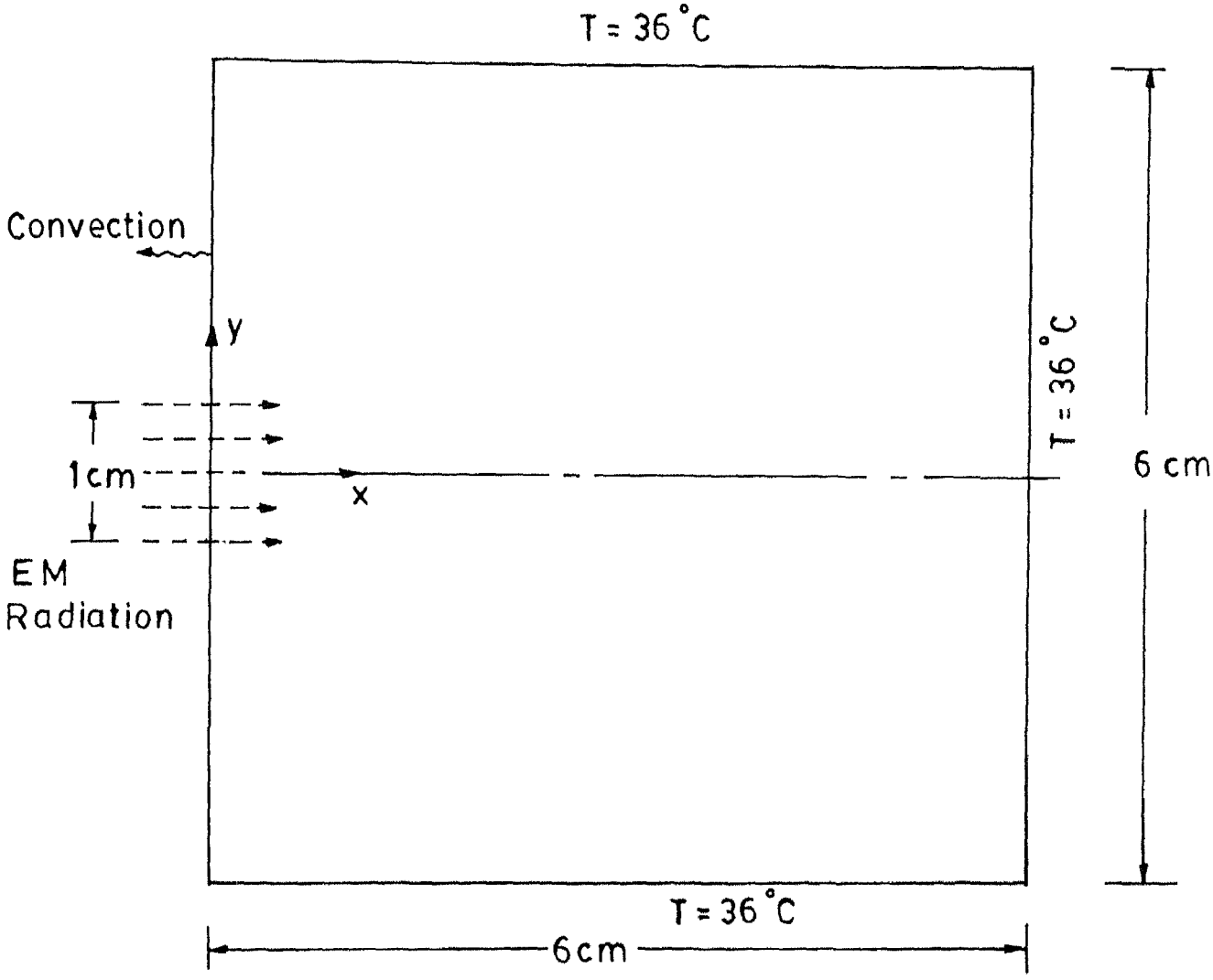

FIG. 2.1 TISSUE REGION CONSIDERED FOR SOLUTION DOMAIN

Table 2.1 : Value of the Thermal, Electrical and Magnetic Properties for Air, Muscle, Lung and Blood

For Air or Vacuum:

$\mu_o = 4 \times 10^{-7}$ $N\text{-}S^2/C^2$

$\gamma_o = 0.8854 \times 0^{-11}$ $C^2/N\text{-}m^2$

For Muscle and Lung:

$C_{Pt} = 2.925.0$ $J/kg\text{-}^oC$

$\rho_t = 1000.0$ Kg/m^3

$K_t = 0.625$ $W/m\text{-}^oC$

$\mu_r = 1.0$

For Muscle only:

$\gamma_r = 128$

$r_e = 1.5873$ Ohm-m

For Lung only:

$\gamma_r = 40$

$r_e = 3.7037$ Ohm-m

For Blood:

$\rho_b = 1000.0$ kg/m^3

$C_{Pb} = 4184.0$ $J/kg\text{-}^oC$

may be expressed by the transient bio-heat transfer equation of the form:

$$K_t \nabla^2 T - W_b C_{pb} (T - T_a) + Q = \rho_t C_{pt} \frac{\partial T}{\partial t} \qquad (2.1)$$

where T is the local tissue temperature, K_t is the tissue thermal conductivity, W_b is the blood perfusion rate, C_{pb} is the specific heat of blood, T_a is the arterial blood temperature (generally considered as constant), Q is the rate of volumetric heat-generation, C_{pt} is the effective specific heat of the tissue, ρ_t is the density of tissue and t is the time of heating.

The above formulation for bio-heat transfer analysis is chosen, because it qualitatively describes the tissue characteristics reasonably well and it provides an adjustable parameter, W_b, that has been identified with the rate of blood perfusion in a real tissue. The blood perfusion term in the above equation acts as a heat sink, which arises from thermal equilibration of the blood in the capillaries with the surrounding tissue. Recent studies, that rigorously relate the blood tissue heat-transfer to the vascular organisation in tissues, have shown that blood thermally equilibrates in relatively large counter-current vessels [5, 6]. They suggest that the bio-heat equation seems to work only because it provides enough adjustable parameters to fit the available data. In any case, for want

of a better model at present to describe tissue hyperthermia, the bio-heat equation has been adopted in the present work.

2.2b INTERACTION OF EM RADIATION WITH DIELECTRIC MEDIA:

The Maxwell's equations which govern the variation of the magnetic and electric field vectors ($\underline{H}$ and $\underline{E}$ respectively) are given by:

$$\nabla \times \underline{H} = \gamma \cdot \frac{\partial \underline{E}}{\partial t} + \frac{\underline{E}}{r_e} \qquad (2.2)$$

$$\nabla \times \underline{E} = -\mu \cdot \frac{\partial \underline{H}}{\partial t} \qquad (2.3)$$

$$\nabla \cdot \underline{E} = 0 \qquad (2.4)$$

$$\nabla \cdot \underline{H} = 0 \qquad (2.5)$$

The properties of electromagnetic waves through any dielectric medium are governed by the Maxwell's equations given above. For simplicity, the following restrictions are imposed on the electromagnetic radiation to which the biological tissue is exposed:

(i) A plane wave of incident radiation is considered that is propagating in x-direction. All the properties associated with the wave are assumed to be constant over any YZ plane at any given instant of time. Thus,

$$\frac{\partial}{\partial Y} = \frac{\partial}{\partial Z} = 0$$

(ii) The electro-magnetic wave is polarized such that the electric field vector $\underline{E}$ is contained only in the X-Y plane and the magnetic field vector $\underline{H}$ is contained only in the X-Z plane. Thus,

$$E_Z = 0 \quad , \quad E_X = 0$$

$$H_Y = 0 \quad , \quad H_X = 0$$

After incorporating the above-mentioned assumptions in equations (2.2) - (2.5), the general electric and magnetic field equations are obtained as:

$$\frac{\partial^2 E_Y}{\partial X^2} = \mu\gamma \cdot \frac{\partial^2 E_Y}{\partial t^2} + \frac{\mu}{r_e} \frac{\partial E_Y}{\partial t} \qquad (2.6)$$

and

$$\frac{\partial^2 H_Z}{\partial X^2} = \mu\gamma \cdot \frac{\partial^2 H_Z}{\partial t^2} + \frac{\mu}{r_e} \frac{\partial H_Z}{\partial t} \qquad (2.7)$$

Equations (2.6) and (2.7) can be identified as the wave equations that describe the propagation of the electrical and magnetic component in the x-direction for an isotropic medium of finite electrical conductivity.

Analytical solution for equation (2.6) is:

$$E_y = E_{YM}\left[\exp\ i\omega\left(t - \frac{n}{C_o} x\right)\right] \exp\left(-\frac{\omega}{C_o} KX\right) \qquad (2.8)$$

and that for equation (2.7) is:

$$H_Z = H_{ZM} \exp\left[i\omega\left(t - \frac{n}{C_o} X\right)\right] \exp\left(-\frac{\omega}{C_o} KX\right) \qquad (2.9)$$

By observing the above two equations, it is quite obvious that E_Y and H_Z are attenuated exponentially with distance when the radiation passes through an isotropic medium of finite conductivity. The term $\exp(-\frac{\omega}{C_o} KX)$ in both the equations (2.8) and (2.9) causes the attenuation of the electromagnetic field intensities. The complex refractive index, $\bar{n}$, for the dielectric medium is given by:

$$\bar{n} = + n - iK$$

where K is termed the extinction coefficient for that medium as it causes attenuation of the electro-magnetic wave. The values of n and K can be found out from the relations:

$$n^2 = \frac{\mu\gamma C_o^2}{2} \left[1 + \left[1 + \left(\frac{\lambda_o}{2\pi C_o r_e \gamma}\right)^2\right]^{1/2}\right] \qquad (2.10)$$

$$K^2 = \frac{\mu\gamma C_o^2}{2} \left[-1 + \left[1 + \left(\frac{\lambda_o}{2\pi C_o r_e \gamma}\right)^2\right]^{1/2}\right] \qquad (2.11)$$

It can be shown that the relation between E_Y and H_Z is

$$H_Z = \frac{(n - iK)}{\mu C_o} E_Y \qquad (2.12)$$

2.2c ENERGY FLUX DETERMINATION OF THE EM WAVE:

The instantaneous energy carried per unit time and per unit area by an electromagnetic wave is given by

the cross-product of the electric and the magnetic field intensity vectors. This product is known as the Poynting vector $\underline{S}$, given by the expression:

$$\underline{S} = \underline{E} \times \underline{H} \tag{2.13}$$

and according to the properties of the cross-product, $\underline{S}$ is a vector propagating at right angles to the electric and the magnetic field vectors in a direction defined by the right hand rule. For the present case, the magnitude of $\underline{S}$ is given as

$|\underline{S}| = E_Y H_Z$ and the direction of $\underline{S}$ is the same as that of the wave propagation.

Using equation (2.12) in (2.13),

$$|\underline{S}| = \frac{\bar{n}}{\mu C_o} E_y^2 \tag{2.14}$$

Thus the instantaneous energy per unit time per unit area carried by the wave is proportional to the square of the amplitude of electric field intensity.

Considering the real part of E_Y only,

$$E_Y = E_{YM} \cos\left[\omega\left(t - \frac{n}{C_o} X\right)\right] \exp\left(-\frac{\omega}{C_o} KX\right) \tag{2.15}$$

Substituting for E_Y in equation (2.14) from equation (2.15),

$$|\underline{S}| = \frac{\bar{n}}{\mu C_o} E_{YM}^2 \exp\left(-\frac{2\omega KX}{C_o}\right) f(X,t) \tag{2.16a}$$

where,

$$f(X,t) = \left[\cos\left[\omega\left(t - \frac{n}{C_o} X\right)\right]\right]^2 \qquad (2.16b)$$

For the present case, since the electromagnetic radiation is of very high frequency, the instantaneous energy can be averaged over time as:

$$|\underline{S}| = \frac{\bar{n}}{\mu C_o} E_{YM}^2 \exp\left(-\frac{2\omega KX}{C_o}\right) f_{av.}(X,t) \qquad (2.17a)$$

where,

$$f_{av.}(X,t) = \frac{1}{2\pi/\omega} \int_o^{2\pi/\omega} f(X,t)\, dt = \frac{1}{2} \qquad (2.17b)$$

Thus,

$$|\underline{S}| = \frac{\bar{n}}{\mu C_o} \cdot \frac{E_{YM}^2}{2} \exp\left[-\left[\frac{2\omega KX}{C_o}\right]\right] \qquad (2.18)$$

Considering the real part of equation (2.18),

$$|\underline{S}| = \frac{n}{\mu C_o} \cdot \frac{E_{YM}^2}{2} \exp\left[-\frac{2\omega KX}{C_o}\right] \qquad (2.19)$$

The extinction coefficient exists only for an electromagnetic wave passing through an isotropic medium of finite electrical conductivity. For the electromagnetic wave passing through air or vacuum, since these media can be assumed to possess infinite electrical resistivity (i.e. $r_e = \infty$), the extinction coefficient K is zero and

hence there is no attenuation term in the analytical solution for the electric and the magnetic field intensities. In such a case:

$$E_{Y,0} = E_{YM} \cos\left[\omega\left(t - \frac{n}{C_o} X\right)\right] \qquad (2.20a)$$

and

$$H_{Z,0} = H_{ZM} \cos\left[\omega\left(t - \frac{n}{C_o} X\right)\right] \qquad (2.20b)$$

where $E_{Y,0}$ and $H_{Z,0}$ are the field intensities in air or vacuum. The instantaneous flux of an electro-magnetic wave, while passing through air, is then given by

$$|\underline{S}|_o = \frac{1}{\mu_o C_o} \frac{E_{YM}^2}{2} = S_o \text{ (CONSTANT)} \qquad (2.21)$$

For the present problem, $|\underline{S}_o|$ is nothing but the energy of the incident electromagnetic radiation before entering the tissue region of interest.

2.2d CALCULATION OF THE RATE OF HEAT GENERATION PER UNIT VOLUME:

As the electromagnetic wave penetrates the biological tissue, due to the inherent dielectric properties of the tissue medium, some portion of the energy carried by the wave is absorbed within the tissue. This rate of energy absorption per unit volume of the tissue is given by:

$$Q = -(\nabla \cdot \underline{S}) \tag{2.22}$$

Since $\underline{S}$ exists only in x-direction,

$$Q = -\frac{\partial}{\partial x}(|\underline{S}|) = -\frac{\partial}{\partial x}\left[\frac{n}{\mu C_o}\ \frac{E_{YM}^2}{2}\ \exp\left(-\frac{2\omega KX}{C_o}\right)\right] \tag{2.23}$$

The negative sign in the above expression arises due to the fact that $|\underline{S}|$ decreases in the positive x-direction. Thus,

$$Q = \frac{\omega n K}{\mu C_o^2}\ E_{YM}^2 \cdot \exp\left(-\frac{2\omega KX}{C_o}\right) \tag{2.24}$$

Using equation (2.21) in equation (2.24),

$$Q = Q_o\ \left(\frac{nK}{\mu_r}\right) \cdot \exp\left(-\frac{2\omega KX}{C_o}\right) \tag{2.25}$$

where,

$$Q_o = \frac{2\omega S_o}{C_o}.$$

It is noted from equation (2.25) that the volumetric rate of heat-generation depends upon so many factors like Q_o, n, K, μ_r etc. Q_o is a dimensional parameter independent of the di-electric medium and is dependent only upon the energy and the frequency of the incoming wave.

2.2e GOVERNING EQUATIONS:

After substitution of Q from equation (2.25) the bio-heat equation (2.1) can be rewritten as follows:

$$K_t \nabla^2 T - W_b C_{pb} (T - T_a) + Q_o \left(\frac{nK}{\mu_r}\right) \exp\left(-\frac{2\omega KX}{C_o}\right) = \rho_t C_{pt} \frac{\partial T}{\partial t} \qquad (2.26)$$

Boundary Conditions:

Here, the heat transfer analysis is performed over a region which is sufficiently large compared to the dimension of the irradiated area. The boundary conditions that have been used for the four faces of the solution domain (Fig. 2.1) are those of convective heat loss to the atmosphere and known boundary temperatures. For the face which is exposed to the atmosphere, convective boundary condition has been applied in the form:

$$K_t \frac{\partial T}{\partial X} = h(T - T_f) \text{ at } X = 0 \text{ and } 0 \leq Y \leq L \qquad (2.27a)$$

Since the portion, which experiences the effect of hyper-thermia, is small compared to the whole region, the three faces of the region at Y = 0, Y = L and X = L can be considered to be at the body temperature. Thus,

$$X=L, \quad 0 \leq Y \leq L \text{ for all } t \tag{2.27b}$$

$$T=T_a \text{ for } Y=0, \quad 0 \leq X \leq L \text{ for all } t \tag{2.27c}$$

$$Y=L, \quad 0 \leq X \leq L \text{ for all } t \tag{2.27d}$$

Initial Condition:

Prior to the exposure to microwave heating, the entire tissue region is assumed to be at normal arterial temperature. Thus,

$$T = T_a$$

$$\text{at } t=0 \text{ for } 0 \leq x \leq L \text{ and } 0 \leq Y \leq L \tag{2.27e}$$

2.3 DETERMINATION OF BLOOD PERFUSION RATE:

In the present study, the blood perfusion rate has been estimated in the following manner:

(i) Firstly, the blood perfusion rate has been considered to be constant with time and unaffected by the tissue temperature. In this case, blood perfusion rate has been varied from 1 kg/m^3s to 7.0 kg/m^3s, independent of the SAR (Specific Absorption Rate) value.

(ii) In the second approach, the blood perfusion rate has been considered to vary with time and tissue temperature. This assumption is much more realistic in nature. The temperature control system inside the human body has a very complex behaviour. The body tries to restore

the temperature to the normal value of $36^{o}C$, whenever it decreases or increases. This is done partly by varying the blood perfusion rate and partly by other mechanisms such as perspiration. Generally blood perfusion rate increases with the increase in tissue temperature. This control of blood perfusion rate for different tissue temperature is done by the brain through biological feed-back control mechanism. There is always some time-lag for the signal to reach the proper destination. Hence, blood perfusion rate is also a function of time.

The nature of dependence of blood perfusion rate on time and temperature has been taken from [10]. Here simple linear interpolation and extrapolation have been used to find out the blood perfusion rate corresponding to a given average tissue temperature at a given time from the data presented in Table 2.2. These blood perfusion data for human thigh muscles of persons having an average build, are shown in Table 2.2.

2.4 NON-DIMENSIONALISATION OF THE GOVERNING EQUATIONS:

The bio-heat equation has been non-dimensionalised using the following dimensionless variables:

$$X^{*} = \frac{X}{L}\ ,\ Y^{*} = \frac{Y}{L}\ ,\ T^{*} = \frac{T - T_{a}}{T_{a} - T_{amb}}$$

$$t^{*} = \frac{t}{L^{2}/\alpha_{t}}\ .$$

Table 2.2 : Variation of Blood Perfusion Rate with Tissue Temperature and Time for Human Thigh Muscle [10]

Temp. (°C) / Time (Min)	30	31	32	33	34	35	36	37	38	39	40	41	42	43	44	45
0					0.55 125	0.55 125	0.55 125									
10	0.551 25	0.556	0.574 2187	0.592 5937	0.611	0.60 6371	0.56 9625	0.56 9625	0.56 9625	0.56 9625	0.56 9625					
15	0.648 375	0.662	0.676 43	0.69	0.704	0.71 77	0.73 15	0.735	0.73 5	0.73 5	0.73 5	0.735	0.86 36	0.99 2	1.47	
17	0.612	0.622	0.632 8	0.643	0.659	0.66 4	0.675	0.685	0.69 6	0.827	1.00 4	1.257 8	1.587 5	2.12 187	2.8656	4.584 56
24	0.699	0.699	0.699	1.777	1.654	2.13 17	2.609	3.086	3.56 355	4.04 08	4.9 38	6.817	7.083	7.35		

Unit of Blood Perfusion Rate: kg/m^3-s

Equation (2.26), can then be rewritten as:

$$\nabla^2 T^* + Q^* \exp(-BX^*) - W^* T^* = \frac{\partial T^*}{\partial t^*} \qquad (2.28)$$

where,

$$Q^* = \frac{Q_o L^2}{K_t (T_a - T_{amb})} \times \frac{nK}{\mu_r} \qquad (2.28a)$$

$$W^* = \frac{W_b}{K_t/(C_{pb} L^2)}, \quad B = \frac{2\omega KL}{C_o} \qquad (2.28b)$$

and,

$$Q_o = \frac{2\omega S_o}{C_o} . \qquad (2.28c)$$

The non-dimensional initial and boundary conditions are:

(i) $T^* = 0$ at $t^* = 0$ for $0 \leq X \leq 1$ and $0 \leq Y^* \leq 1$ (2.29a)

(ii) $$\frac{\partial T^*}{\partial X^*} = \frac{hL}{K_t} \left[T^* - \frac{(T_f - T_a)}{(T_a - T_{amb})} \right] = Bi[T^* - T_f^*]$$

at $X^* = 0$ and $0 \leq Y^* \leq 1$ (2.29b)

(iii) $T^* = 0$ at $X^* = 1$ and $0 \leq Y^* \leq 1$ (2.29c)

(iv) $T^* = 0$ at $Y^* = 0$ and $0 \leq X^* \leq 1$ (2.29d)

(v) $T^* = 0$ at $Y^* = 1$ and $0 \leq X^* \leq 1$ (2.29e)

CHAPTER 3

FINITE ELEMENT ANALYSIS

3.1 INTRODUCTION:

The solution procedure that has been used for the present study is the finite element method. There are many advantages of using FEM as the solution procedure for the hyperthermia analysis. First of all, it can handle any complex geometrical shape of the tissue being irradiated. The heating or cooling boundary conditions for the tissue of interest may be introduced in a very general manner. Material property variation with location can be very easily accounted for. In view of the above mentioned generality and flexibility provided by FEM solution technique, it has been employed for solving the present problem.

3.2 DESCRIPTION OF THE FEM SOLUTION PROCEDURE BY GALERKIN APPROACH:

In FEM, the solution domain which is continuous, is divided into several subregions each of which is known as an element. Each of these elements is of chosen shape and a prescribed number of nodes are placed within and on the boundary of each element. The collection of elements within the entire solution domain is called the finite element mesh. The solution variables are approximated [Fig.3.1]

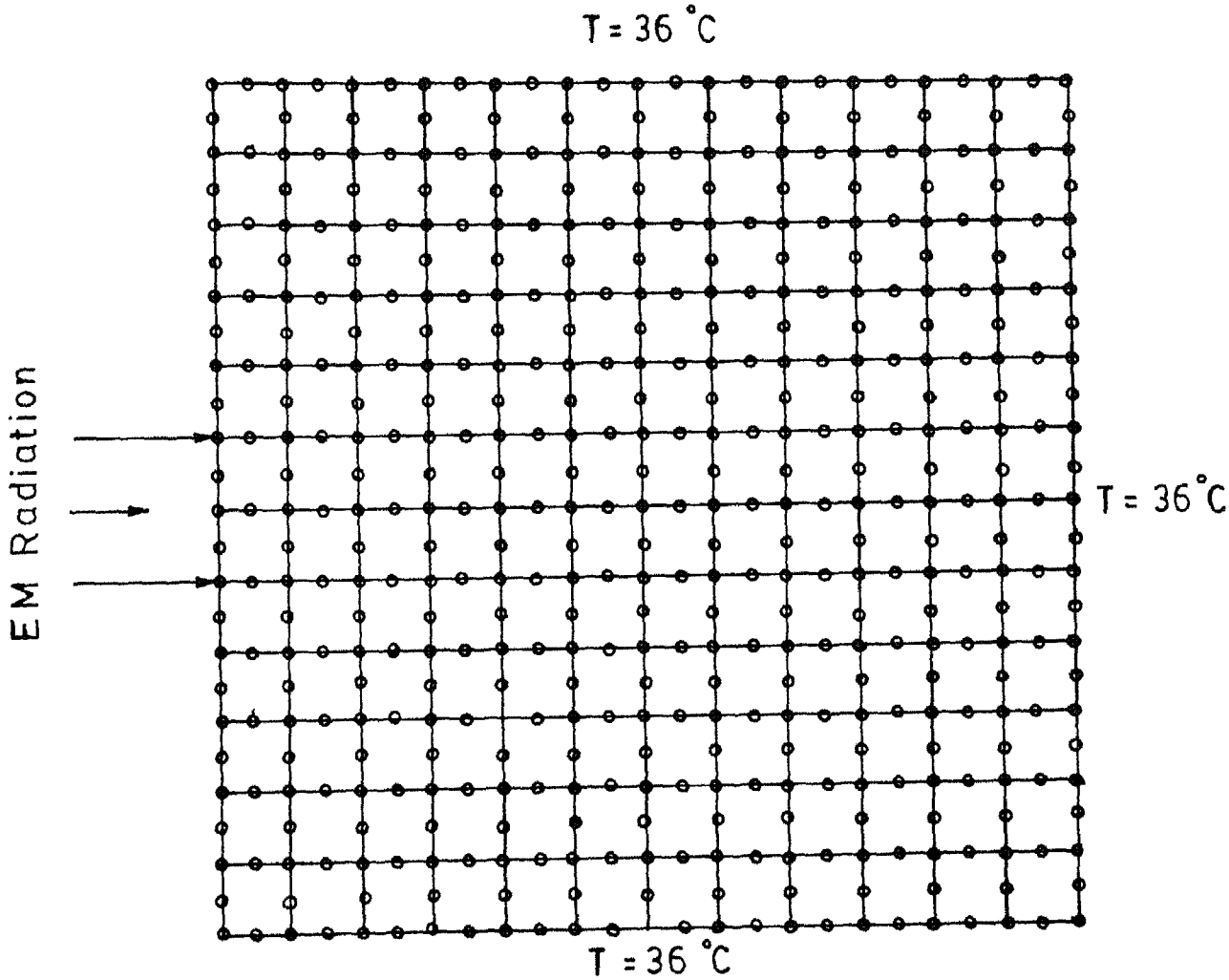

FIG. 3.1 FINITE ELEMENT MESH FOR THE SOLUTION DOMAIN

within each element by suitable approximating functions. The error in satisfying the governing equations is minimised in an integral sense over the whole domain leading to the formulation of a set of simultaneous algebric equations for all the nodal variables. Finally, the solution of these nodal equations gives the required solution. The above steps can be summarised as follows:

(a) The equivalent integral equations are obtained from the governing differential equations by minimising the error in satisfying the governing equations in an integral sense over the whole domain.

(b) The continuous solution domain is divided into a number of elements with a chosen number of nodes placed at desired locations within each element. All the elements can be of the same shape or of different shapes. A mesh-generation program may be used to obtain the finite-element-mesh [Fig.3.1].

(c) Each governing integral equation over the solution domain is written as a sum of the integral over all the elements.

(d) A typical element is isolated and the approximating functions for describing the field variables are obtained within that element in terms of their nodal values. For this element, firstly, the elemental integrals are evaluated leading to the formation of an elemental coefficient matrix and elemental right hand side vector. Then the boundary

integrals (if any) are evaluated to obtain the boundary coefficient matrix and the boundary right hand side vector. These elemental and boundary coefficient matrices assembled for each element to obtain the final form of the elemental coefficient matrix. A similar operation is done for the elemental right hand side vector also.

(e) The elemental coefficient matrices are then assembled for all the elements, giving rise to a global coefficient matrix. The elemental right hand side vectors are also assembled leading to the formation of the global right hand side vector.

(f) The matrix equations obtained in the previous step are solved to find the unknown field variables at all the nodes.

3.3 METHOD OF WEIGHTED RESIDUALS:

Weighted residual methods are, in essence, numerical techniques which can be used to solve a set of partial differential equations. The first step in the application of the weighted residual procedure is to assume that the unknown variable, ϕ, can be approximated over the whole domain by

$$\phi^* = \sum_{i=1}^{n} N_i \phi_i \qquad (3.1)$$

where N_i are the interpolation functions described in terms of the spatial coordinates (X, Y) and $\emptyset_i$ are the values of $\emptyset$ at certain chosen locations.

Consider the equation:

$$\mathcal{L}(\emptyset) = 0 \qquad (3.2)$$

where $\emptyset$ is the exact solution of the differential operator. An approximate solution, $\emptyset^*$, given by eq. (3.1) gives rise to an error or residue R while substituted into eq. (3.2), such that

$$R = \mathcal{L}(\emptyset^*)$$

In the weighted residual methods R is minimised over the whole solution domain in the integral sense with a set of arbitrary 'weighting functions', W_i, such that over the whole domain, D,

$$\int_D W_i \, R \, d \, D = 0 \qquad (3.3)$$

where $i = 1,2,\ldots.n$.

If the number of unknown values of $\emptyset$ is n, then by using n linear independent weighting functions enough equations can be generated to solve all the unknowns. The only limitation, at this stage, placed on W_i, is that they must be positive, single-valued and finite.

The Galerkin's Method is a very special case of the method of weighted residuals, where the weighting functions, W_i, are taken to be the same as the interpolation functions, N_i, which are more commonly known as shape functions .

Therefore, for Galerkin's Method, the residue minimization equations can be written as:

$$\int_D N_i \mathcal{L}(\phi^*) \, d\,D = 0$$

where,

$$\phi = \sum_{j=1}^{n} N_j \phi_j \qquad (3.4)$$

3.4 APPLICATION OF FEM TO BIO-HEAT-TRANSFER EQUATION:

The dimensionless bio-heat-transfer equation (with the stars omitted for convenience) is given as:

$$\nabla^2 T - WT + Q \exp(-BX) = \frac{\partial T}{\partial t} \qquad (3.5)$$

Applying the Galerkin method to this equation, we obtain the residue minimisation equation as:

$$\iint_A N_i \frac{\partial T}{\partial t} \, dX dY - \iint_A N_i \nabla^2 T \, dX \, dY - \iint_A N_i Q e^{-BX} \, dX \, dY$$

$$+ \iint_A N_i WT \, dX \, dY = 0 \qquad (3.6)$$

The unknown variable, T, can be expanded in terms of its nodal values and shape functions as:

$$T = \sum_{j=1}^{n} N_i \, T_j \qquad (3.7)$$

where n is the number of nodes per element.

Using equation (3.7) in equation (3.6) and applying integration by parts to the second term of eqn. (3.6), we obtain:

$$[\iint N_i \, N_j \, dX \, dY] \, \{\dot{T}_j\} + [\frac{1}{K_t} \oint_B N_i \, (-K_t \, \frac{\partial T}{\partial n}) \, dl \,]$$

$$+ [\iint (\frac{\partial N_i}{\partial X} \cdot \frac{\partial N_j}{\partial X} + \frac{\partial N_i}{\partial Y} \cdot \frac{\partial N_j}{\partial Y}) \, dX \, dY \,] \, \{T_j\}$$

$$- [Q \iint N_i \, e^{-BX} \, dX \, dY] + [W \iint N_i N_j \, dX \, dY \,] \{T_j\}$$

$$= 0 \qquad (3.8)$$

where $\frac{1}{K_t} \oint_B N_i \, (-K_t \, \frac{\partial T}{\partial n}) \, dl$ is the boundary contribution to the whole domain.

In the above equation, the summation, Σ, has been dropped by adopting the convention that summation is implied if a subscript is repeated.

In the present study, 8-noded iso-parametric elements have been used [See Fig. 3.1] . For isoparametric elements, the global coordinates (X, Y) of a point inside

an element can be expressed in terms of nodal coordinates and shape functions as it has been done for the field variables. Therefore,

$$X = \sum_{i=1}^{8} N_i X_i \qquad (3.9)$$

$$Y = \sum_{i=1}^{8} N_i Y_i \qquad (3.10)$$

The shape functions N_i for the 8-noded iso-parametric element in terms of local coordinates ξ and η, are given by the following relations.

For corner nodes:

$$N_i = \frac{1}{4}(1 + \xi_i \xi)(1 + \eta_i \eta)(\xi_i \xi + \eta_i \eta - 1) \qquad (3.11)$$

For mid-nodes:

$$N_i = \frac{1}{2}(1 - \xi^2)(1 + \eta_i \eta) \text{ for } \xi_i = 0 \qquad (3.12)$$

$$N_i = \frac{1}{2}(1 - \eta^2)(1 + \xi_i \xi) \text{ for } \eta_i = 0 \qquad (3.13)$$

Substituting equations (3.9) - (3.13) in equation (3.8), the final form of the assembled matrix equations are:

$$[\text{GMASS}]\{\dot{T}_j\} + [\text{GCON}]\{T_j\} = \{\text{GGEN}\} \qquad (3.14)$$

where [GMASS] is the global transient matrix, [GCON] is the global coefficient matrix, { GGEN} is the global right hand side vector.

In terms of shape functions or their derivatives, these matrices and vector are expressed as:

$$[\text{GMASS}] = \sum_{e=1}^{m} \iint_{(e)} N_i N_j \, dX \, dY \qquad (3.15)$$

$$[\text{GCON}] = \sum_{e=1}^{m} \left[W \iint_{(e)} N_i N_j \, dX \, dY + \iint_{(e)} \left(\frac{\partial N_i}{\partial X} \cdot \frac{\partial N_j}{\partial X} + \frac{\partial N_i}{\partial Y} \cdot \frac{\partial N_j}{\partial Y}\right) dX dY \right.$$

$$\left. + \; C2 \int_{(e)} N_i \, N_j \, dl \right] \qquad (3.16)$$

$$\{\text{GGEN}\} = \sum_{e=1}^{m} \left[Q \iint_{(e)} e^{-BX} \, N_i \, dX dY + C1 \int_{(e)} N_i \, dl \right] \qquad (3.17)$$

with $C1 = -q^*$ for heat flux condition (3.18a)

$= Bi \; T_f^*$ for convective B.C. (3.18b)

and $C2 = 0$ for heat flux condition (3.19a)

$= Bi$ for convective B.C. (3.19b)

where $q^* = \dfrac{q_t L}{K_t (T_a - T_{amb})}$

Here the line integrals with coefficients C1 and C2 arise due to boundary conditions.

The equation (3.8) represents a set of simultaneous first-order ordinary differential equations of the variable T and its time derivatives.

Here the finite difference technique has been adopted to approximate the time derivatives. This leads to the final matrix equations of the form:

$$[A] \{T\} = \{C\} \tag{3.20}$$

There are three major schemes for handling the time derivatives in the finite-difference technique, namely:

i) Implicit scheme

ii) Explicit scheme

iii) Crank-Nicholson scheme.

Applying a generalised scheme which considers a fraction of the explicit scheme and a fraction of the implicit scheme, eq. (3.14) can be rewritten as,

$$[[GMASS] + \theta \Delta t [GCON]] \{T_j\}^{K+1}$$

$$= [[GMASS] - (1 - \theta)\Delta t [GCON]]\{T_j\}^{K}$$

$$+ \{GGEN\}\Delta t \tag{3.21}$$

The three schemes mentioned above can be obtained

from eqn. (3.21) by assuming different values of the fraction. For instance,

$\theta = 0$ for explicit scheme

$\theta = 0.5$ for Crank-Nicolson scheme

$\theta = 1.0$ for implicit scheme.

Since the implicit scheme is the most stable one and has no restriction as far as the time step is concerned, it has been used in the present study.

For implicit scheme, equation (3.21) simplifies to the form:

$$[[GMASS] + \Delta t[GCON]]\{T_j\}^{K+1} = [GMASS]\{T_j\}^{K} + \{GGEN\}\Delta t \qquad (3.22)$$

Equation (3.22) can be solved to obtain the temperature vector at the (K+1)th time level, knowing the temperature vector at the Kth time level.

3.5 MATRIX SOLUTION PROCEDURE:

Here the Frontal solution method has been used to solve the assembled matrix equations. It is a well-known fact that the method adopted for solving the assembled matrix equation has a significant bearing on the computer storage requirement and execution time when the total number

of unknown variables is very large. It becomes very time consuming and the core memory problem is very accute when a large number of unknowns are solved by the matrix inversion technique. The Frontal solution technique can handle quite a large number of variables without the problem of large core memory and the computer execution time is also quite less.

The Frontal solution technique used in the present work is based on the direct Gaussian elimination procedure for solving the symmetric matrices where the leading diagonal is always used as a pivot. For unsymmetric matrices encountered in a wide range of engineering problems, the most suitable pivot is not necessarily on the leading diagonal and a Frontal solution routine exists for off diagonal pivoting [20] . But since this tends to be more time consuming, the method used in the present work uses only diagonal pivoting and incorporates many features of the Frontal method for solving symmetric matrices.

The overall Frontal solution technique covers the following steps:

i) Formation of the elemental matrices.

ii) Assembling into a small, temporary global matrix of chosen size.

(iii) Introduction of known variable boundary condition.

(iv) Reduction of the global matrix using Gaussian elimination procedure.

(v) Back substitution.

The primary objective of the Frontal method is the elimination of variables as soon as possible after their introduction, via appropriate equations, into the global matrix. When the contributions from all the elements to a particular node point have been assembled, the corresponding variables associated with that node can be eliminated. The complete matrix is, therefore, never assembled, since the reduced equations can be eliminated from the core and stored on disc. The equations held in core, with the corresponding nodes and variables, are termed as the FRONT and the number of unknown variables in the front is termed as the FRONT WIDTH.

The Front width changes continuously, since, if the nodal matrix contribution have been fully summed the corresponding equation reduction based on the diagonal pivot can be executed.

For a non-symmetric global matrix, a preassigned global matrix core area is filled from contributing elements, the largest diagonal entry in the pre-assigned core is then

found and used as the pivot in a direct Gaussian elimination process. As the maximum, predetermined number of equations are eliminated, the corresponding reduced equations are written on to disc and more elements and corresponding equations are taken into core.

The equations, nodes and variables currently in core are termed active, those assigned to disc as deactivated and those yet to appear in core as inactive. This is shown diagrammatically in Fig. (3.2).

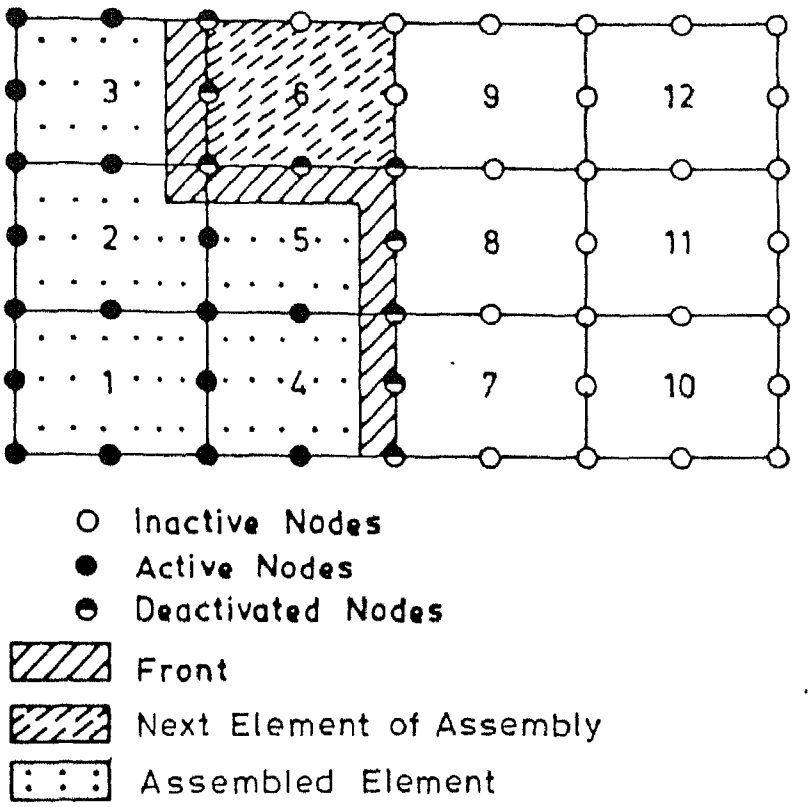

Fig. 3.2 Basic idea of Frontal method.

CHAPTER 4

RESULTS AND DISCUSSIONS

Transient temperature results have been obtained for hyperthermia of human thigh muscle and lung tissue for various SAR values, blood perfusion rates and frequency of radiation. The results are presented in the form of steady state temperature variations with depth, transient temperature variation at the tissue centre and isotherm patterns within the tissue. For checking the validity of numerical results, the special case of hyperthermia with two adiabatic boundaries (Fig. 4.1) and one convective and one prescribed temperature boundaries havebeen considered. Analytical solution exists for the steady state temperature distribution for this case (Appendix A).

In Fig. 4.2, the steady state temperature variation with depth along the centre-line is compared for the analytical and numerical solutions at SAR = 1.0×10^4 W/m^3, W_b = 5.0 kg/m^{3}s and ω = 27 MHz. The two results agree very clearly (within 0.05%), indicating the validity of the present numerical result by FEM.

In Figs. 4.3a, 4.3b and 4.3c, the steady state temperature profiles within the muscle tissue are shown

for various combinations of SAR and W_b. Due to the symmetry of the boundary conditions used in the present formulation, the results are identical about the mid plane of Y = 0. For this reason, in all the three figures, only temperature variation of one half the tissue is shown. Initially, the temperature increases slightly with depth and then decreases gradually and finally drops rapidly to the prescribed boundary temperature of 36°C. The reason for the maximum temperature not occurring at the surface but slightly into the interior is that there is some loss of heat to the atmosphere due to convection at the outer boundary which is exposed to the atmosphere. The gradual decline in temperature with depth is partly because of the decrease in the intensity of the EM wave and partly because of the heat conduction in the lateral direction. The sudden drop in temperature near the inner boundary indicates that the EM radiation is not fully absorbed due to the finiteness of the domain considered. A much larger depth is required to completely dissipate all the EM energy for the parameters assumed for these figures. The figures also indicate that the maximum temperature is achieved along the centre line of the applied radiation, as expected. There is a sharp decrease in temperature in the lateral direction away from the mid-plane and for distances roughly of the order of radiation beam diameter, beyond which the temperature is almost close to the normal body temperature.

Similar trends are observed for all combinations of SAR and W_b, except that for high blood perfusion or low SAR value, there is a small region far away from the tissue mid-plane, along the exposed face where the temperature is below $36^{o}C$. This is because of the convective cooling on the outer boundary.

In Figure 4.4, the temperature profiles along the tissue mid-plane are presented for small time and large time for the thigh muscle. Effects of various combinations of SAR and W_b have also been plotted. It is seen that, at all times, the temperature profiles are similar to the steady state profiles discussed earlier. The graph also indicate that for very large value of SAR or small value of blood perfusion, the temperature levels are high and vice-versa. However, the temperature change is more sensitive to SAR variation than it is to W_b variation. The time taken to reach steady state is found to be higher at larger SAR or lower W_b. This due to the fact that a significant portion of the absorbed energy is carried away by the blood when the steady state is reached. At lower blood perfusion rates, due to the lower heat carrying capacity of the blood, it takes longer time to reach steady state. At higher SAR also, more amount of heat has to be removed by the blood, which takes longer time.

The transient variation of muscle tissue centre temperature is shown in fig. 4.5 for various SAR values at fixed W_b. The steady state value of temperature increases linearly with SAR. This feature is corroborated by the analytical solution of appendix A. The time taken to achieve steady state slightly increases with SAR as discussed earlier.

In fig. 4.6, the variation of muscle tissue centre temperature is plotted with time for different W_b values. The temperature decreases with an increase in blood perfusion as heat sink effect is higher at larger W_b. The steady state temperature (at the tissue centre) varies approximately as $W_b^{-0.6}$. The analytical solution also shows that the dependence of steady state temperatures in the middle portion of the tissue will fall between $1/\sqrt{W_b}$ and $1/W_b$. Because of this, temperature variation is not as sensitive to variation in blood perfusion as it is to the variation in SAR value.

The effect of the EM frequency upon the temperature rise and the heat generated is shown in figs. 4.7a and 4.7b. The surface temperature is essentially insensitive to the radiation frequency, whereas the interior temperature is very much influenced by the frequency of radiation at lower frequency levels. The temperature profile is essentially seen to be governed by the rate of volumetric heat generation

within the tissue (Fig. 4.7b), except near the inner and outer surfaces ,where the applied boundary conditions play an important role. Since the rate of volumetric heat generation decays very steeply with depth and lower amount of heat is generated at high frequencies, the temperature values are also lower and display a strong decay.

The comparison between the mid-plane temperature profiles has been provided for the muscle tissue and the lung tissue in fig. 4.8. The figure shows that the temperature profiles are qualitatively similar for both types of tissue. For the lung tissue, the temperature levels are lower chiefly because of lower dielectric constant. All the other important electric and magnetic properties such as permeability, resistivity etc. are of the same order for both the tissues. It is seen that the decay constant is also lower for the lung tissue.

In Fig. 4.9, the transient temperature variation at the tissue centre is shown for the muscle and the lung tissue. The increase of temperature is seen to be roughly proportional to the dielectric constant. The larger the dielectric constant, the more is the dissipation of energy. The dependence of heat generation on dielectric constant is seen to be linear. The time taken to reach the steady state is larger for the muscle.

Figure 4.10 shows the temperature profiles along the tissue mid-plane for small time and large time for the lung. It essentially shows all the features mentioned for Fig. 4.4 except for the range of temperature variation. The range of temperature variation for lung tissue is much less. This is due to the low value of dielectric constant for lung.

The temperature variation with time at muscle tissue centre is plotted in Fig. 4.11 for automatically varying blood perfusion rate at two different SAR levels. It is seen that the temperature increases rapidly in the beginning and reaches a maximum value at around 18 minutes after the start of heating and then decreases with time. The initial rapid increase in temperature is because of low rates of blood perfusion. However, as the tissue heats up, the temperature-control mechanism is initiated by the brain and the rate of blood perfusion starts increasing with time. As a consequence, the rate of increase of temperature within the tissue is slowed down. After a typical response time of the order of 15 minutes, the temperature starts decreasing due to the already increased value of blood perfusion. The temperature then has a tendency to settle down at a much lower steady state value. It is also seen from the graph that with higher SAR value, the initial rate of temperature increase and the later rate of temperature

decrease are both steeper. The steeper drop of temperature beyond the maximum value occurs due to the larger value of W_b at high temperature.

In Fig. 4.12, the temperature-time response at the muscle tissue centre has been shown for varying blood perfusion and constant blood perfusion models, at a fixed SAR. The fixed W_b model shows a monotonic temperature variation towards the steady state value. This is because of the fact that the heat-sink effect arising from blood perfusion increases linearly with tissue temperature, and at steady state, an equilibrium situation is reached when a significant portion of the supplied heat is removed by blood perfusion. The varying W_b model, on the other hand, has non-linear heat-sink behaviour due to the dependence of W_b on tissue temperature. Since there is also time lag between the rate of temperature increase and the rate of W_b increase, the temperature shoots above the final steady state value.

In Fig. 4.13, the muscle temperature profile for varying W_b are presented for different SAR values. For the sake of comparison, temperature profile with constant W_b is also shown. It is evident from the graphs that the temperature profile is similar for fixed or varying W_b at all SAR levels.

In figures 4.14a,b,c,d, the isotherm plots within the muscle tissue are shown for fixed and varying W_b at two different time levels. The isotherms in the heated region are U-shaped loops indicating that the heat absorbed is mainly conducted away in the lateral direction. The temperature gradient in the axial direction is not very high near the exposed surface. For larger depths, however, the effects of the applied boundary conditions comes into play so that the isotherms near the inner boundary are closely spaced. This features also indicates that all of the applied radiation has not been absorbed within the prescribed depth in the present problem. Far away from the heated region, at some locations near the surface exposed to atmosphere, temperature falls below 36°C because of the convective heat loss to the atmosphere. This consequence occurs because the metabolic heat generation has been neglected in the present work. A comparison of figures 4.14a and 4.14b shows that the temperature profiles are similar at large and small time levels except that heat penetrates to a larger distance for larger time. In the case of varying W_b, at small times, heat penetration is confined to a small region. With increasing time, the entire tissue is heated and some portion of the tissue gets overheated as the variation of blood perfusion rate is still lagging behind. At a still larger time, sufficient increase in blood perfusion has taken place so that the tissue is again cooled. This phenomenon is supported by the Fig. (4.14e).

Thus the numerical results provide both qualitative and quantitative picture of the effects of various parameters during hyperthermia by micro wave radiation.

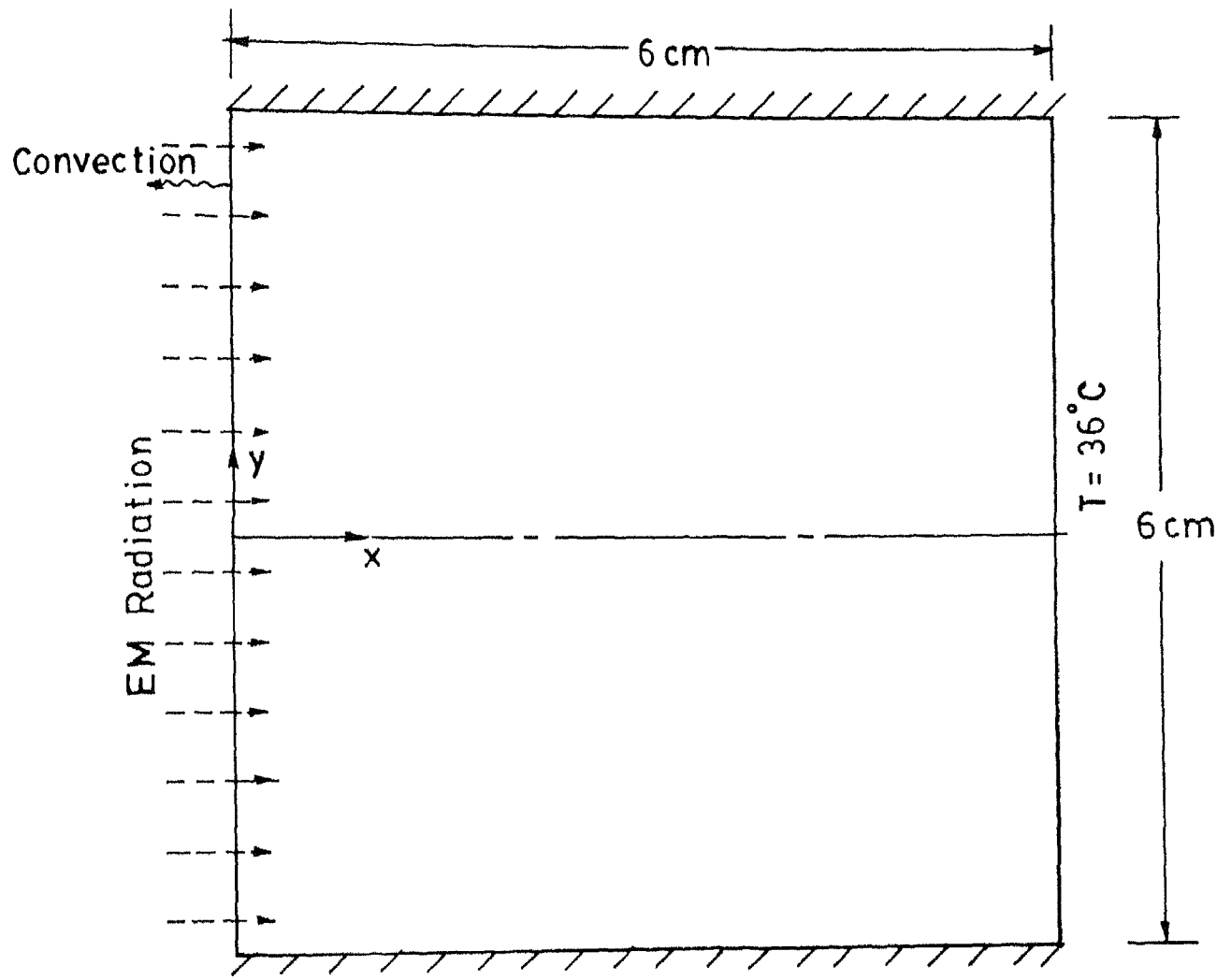

FIG. 4.1 GEOMETRY OF THE TEST PROBLEM

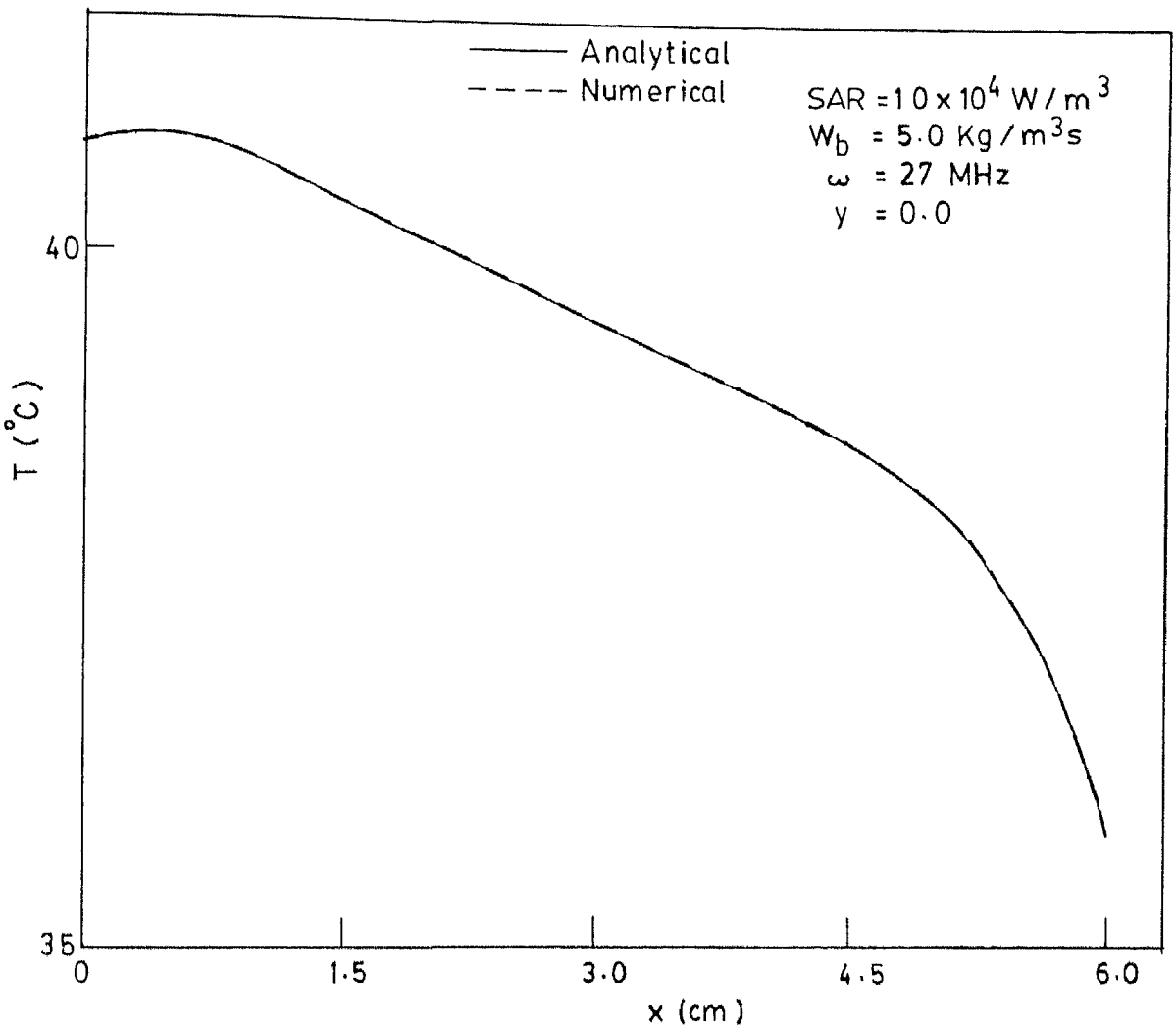

FIG. 4.2 COMPARISON OF NUMERICAL SOLUTION WITH ANALYTICAL SOLUTION FOR A SPECIAL CASE BOUNDARY CONDITION IN MUSCLE

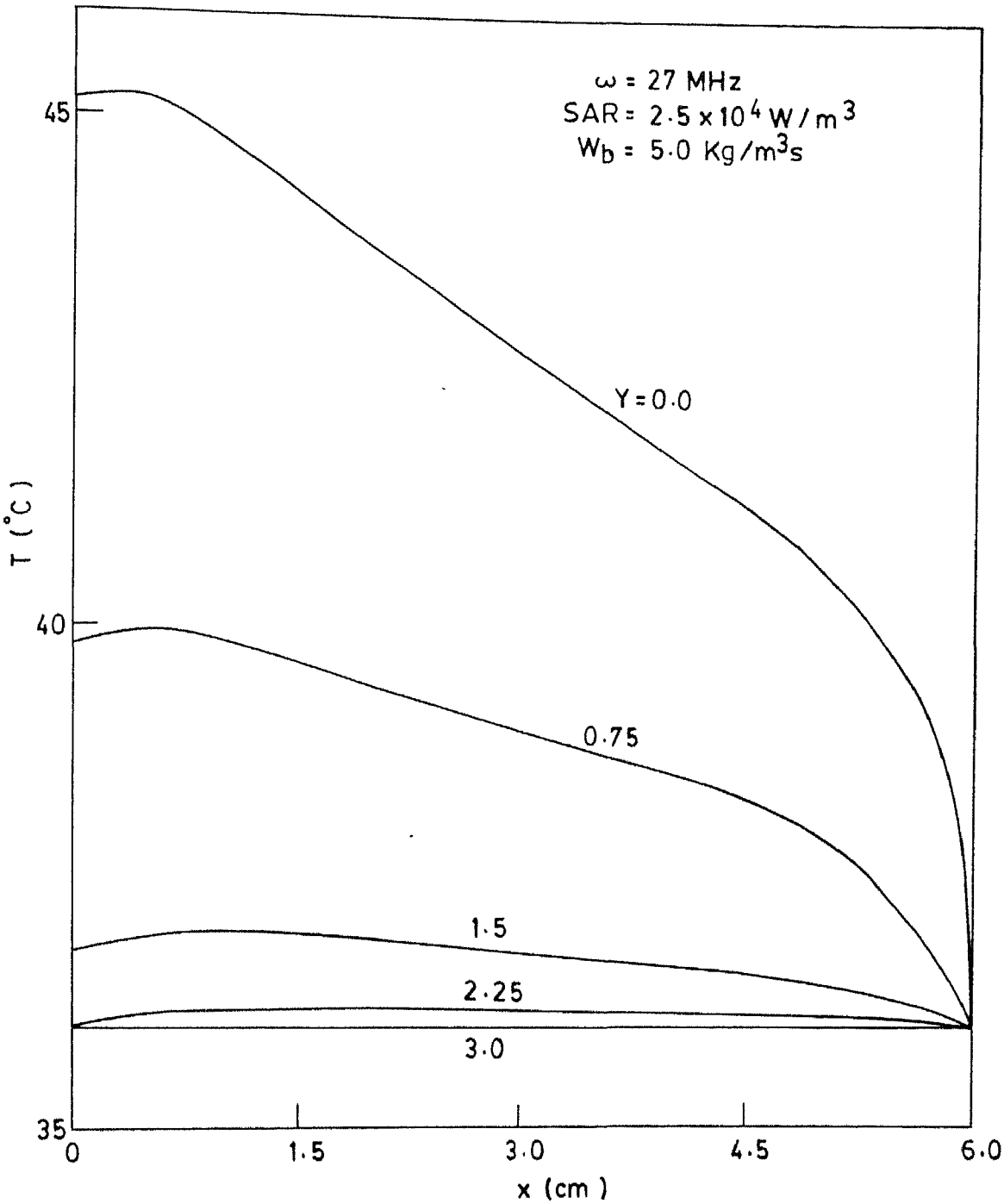

FIG. 4.3a STEADY STATE TEMPERATURE DISTRIBUTION IN THIGH MUSCLE

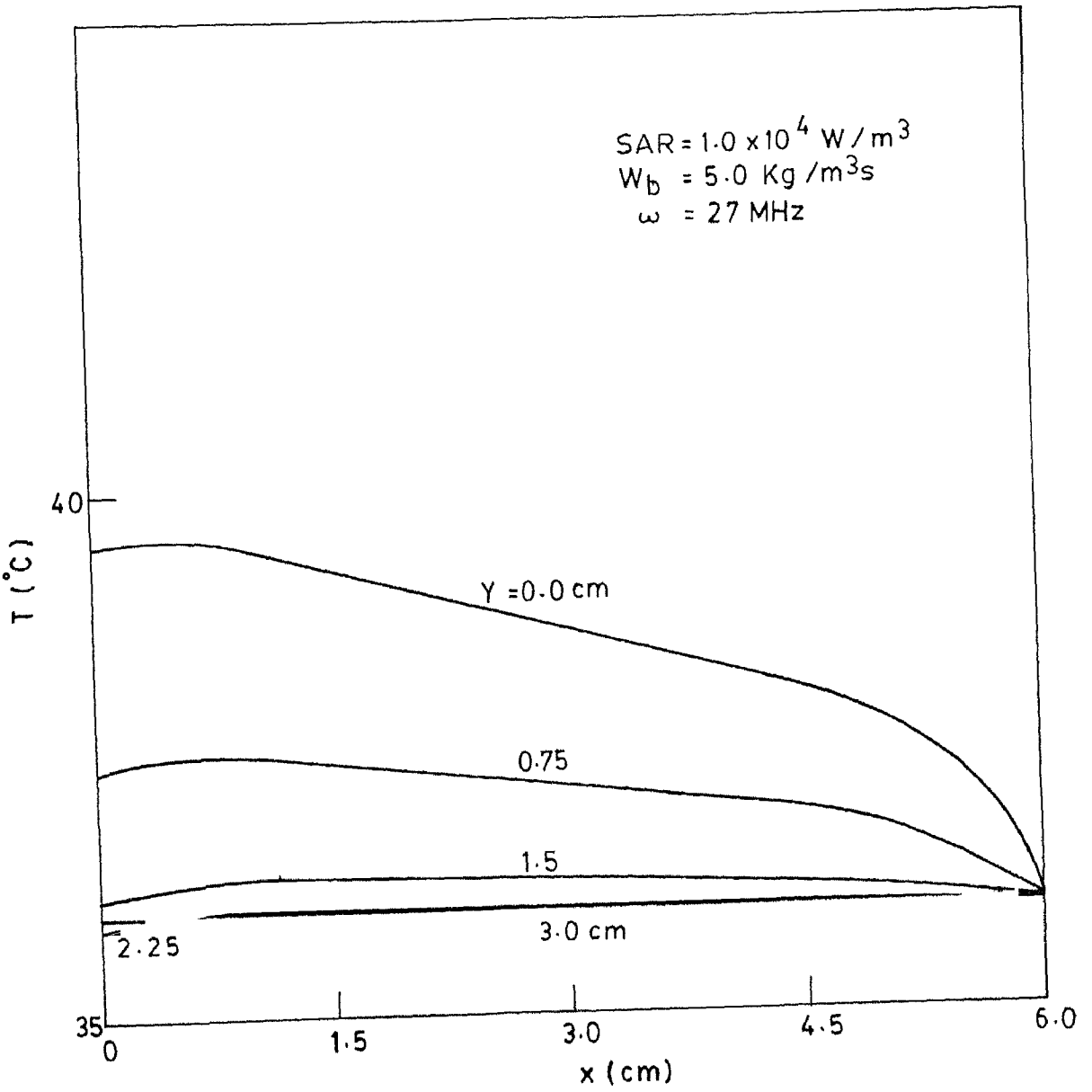

FIG. 4·3b STEADY STATE TEMPERATURE DISTRIBUTION IN THIGH MUSCLE

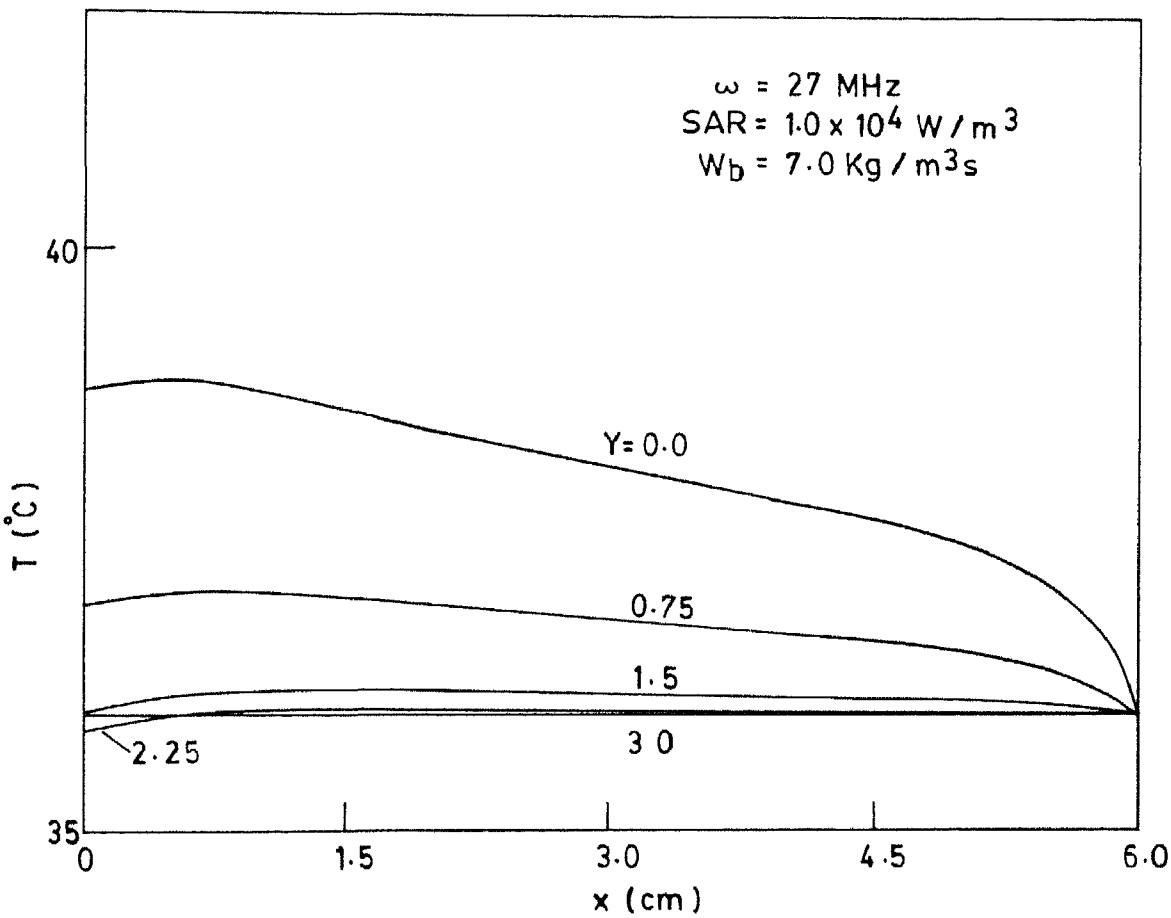

FIG. 4·3c STEADY STATE TEMPERATURE DISTRIBUTION IN THIGH MUSCLE

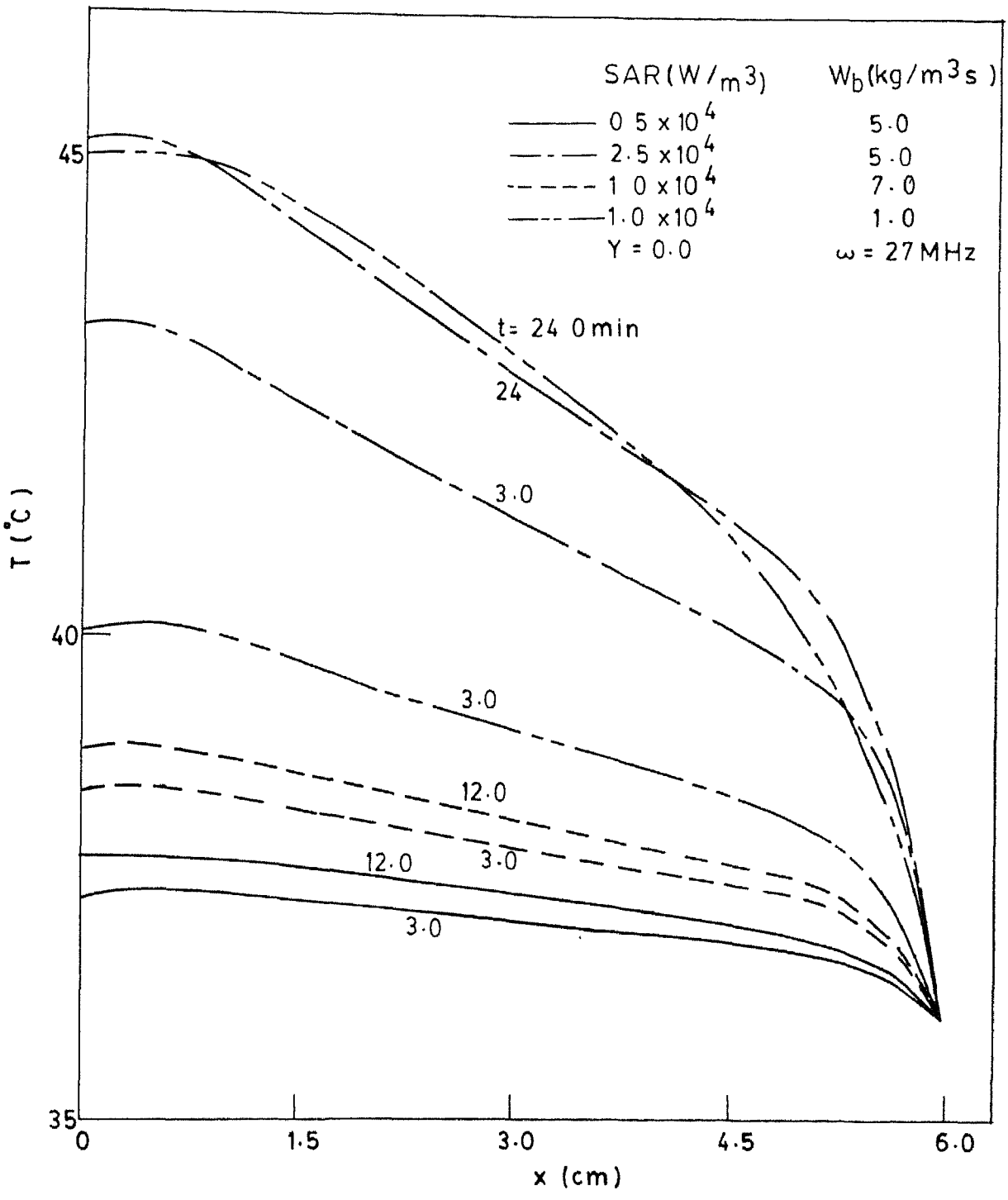

FIG. 4.4 EFFECTS OF SAR AND BLOOD PERFUSION RATE UPON TRANSIENT TEMPERATURE DISTRIBUTION IN THIGH MUSCLE

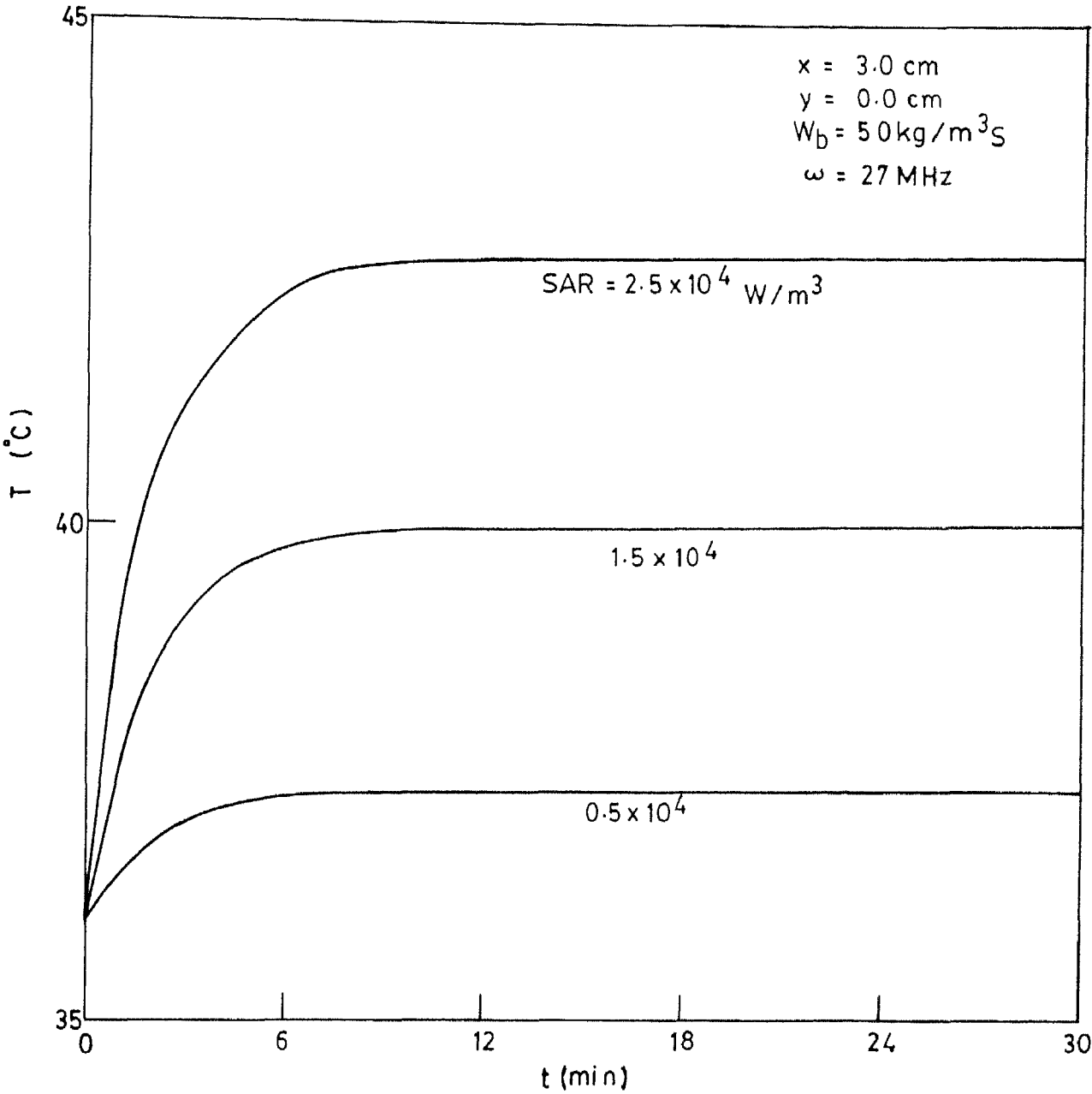

FIG. 4.5 TRANSIENT VARIATION OF MUSCLE CENTRE TEMPERATURE AT VARIOUS POWER LEVELS

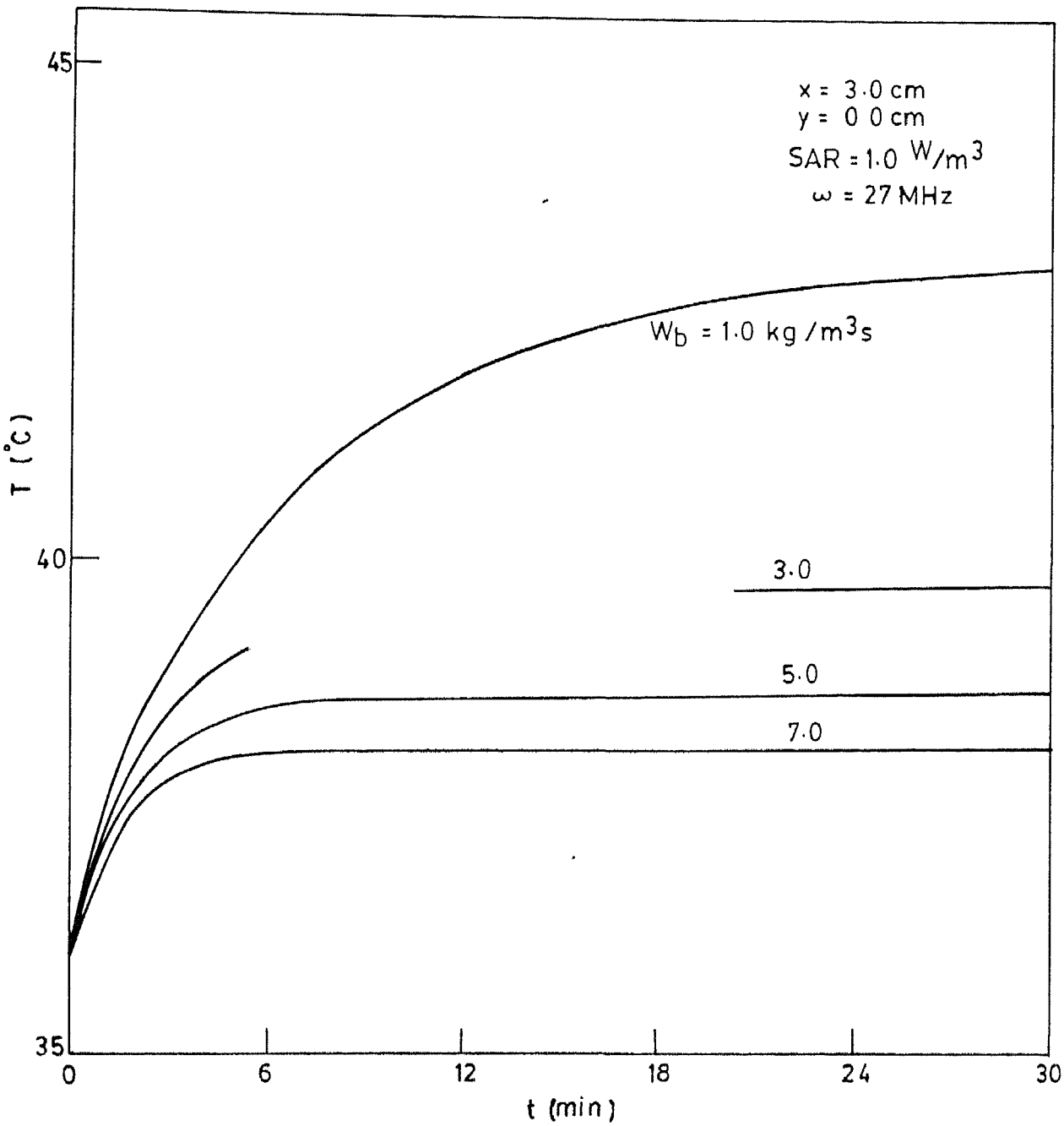

FIG. 4.6 TRANSIENT VARIATION OF MUSCLE CENTRE TEMPERATURE AT DIFFERENT BLOOD PERFUSION RATES

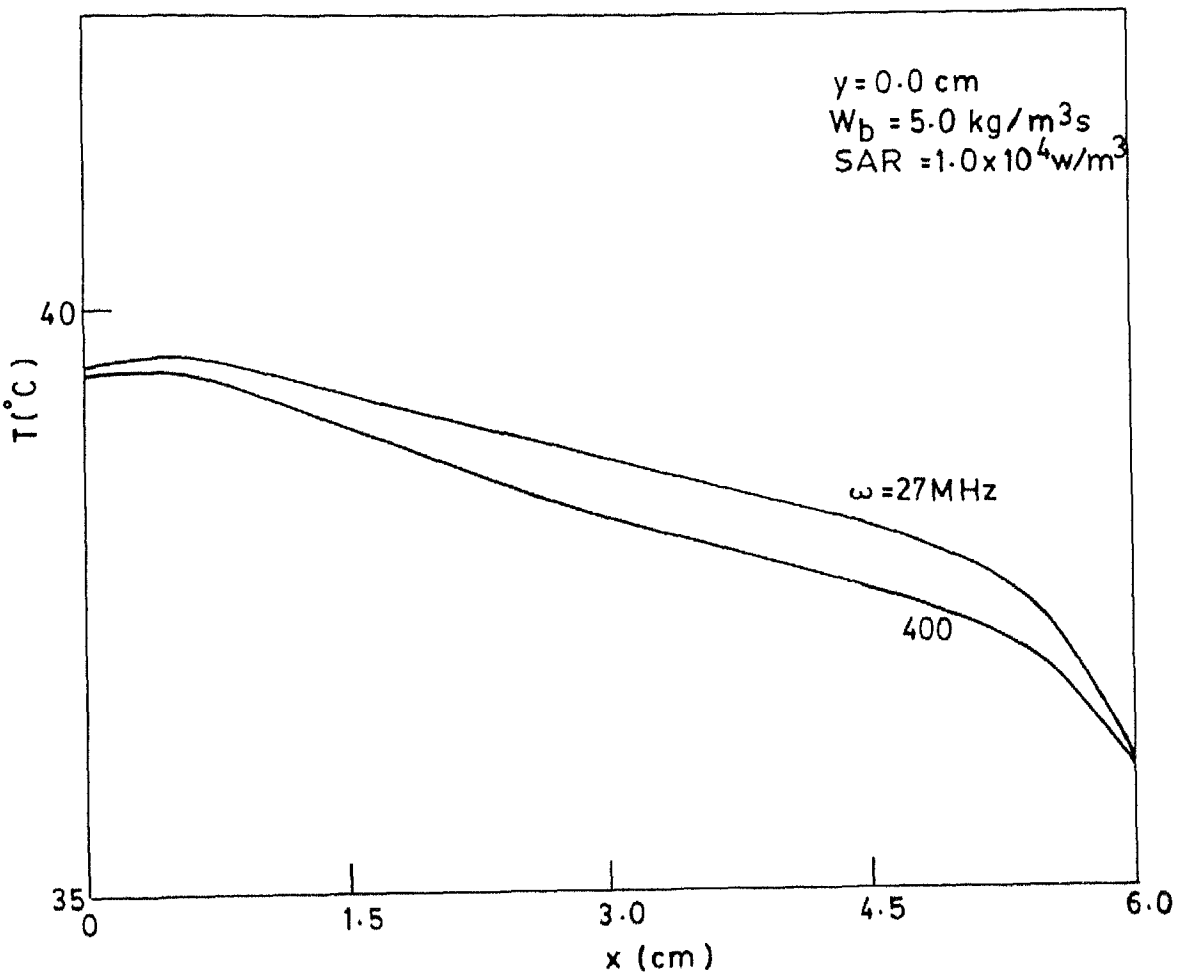

FIG. 4.7a EFFECT OF RADIATION FREQUENCY ON STEADY STATE TEMPERATURE PROFILE OF THE MUSCLE

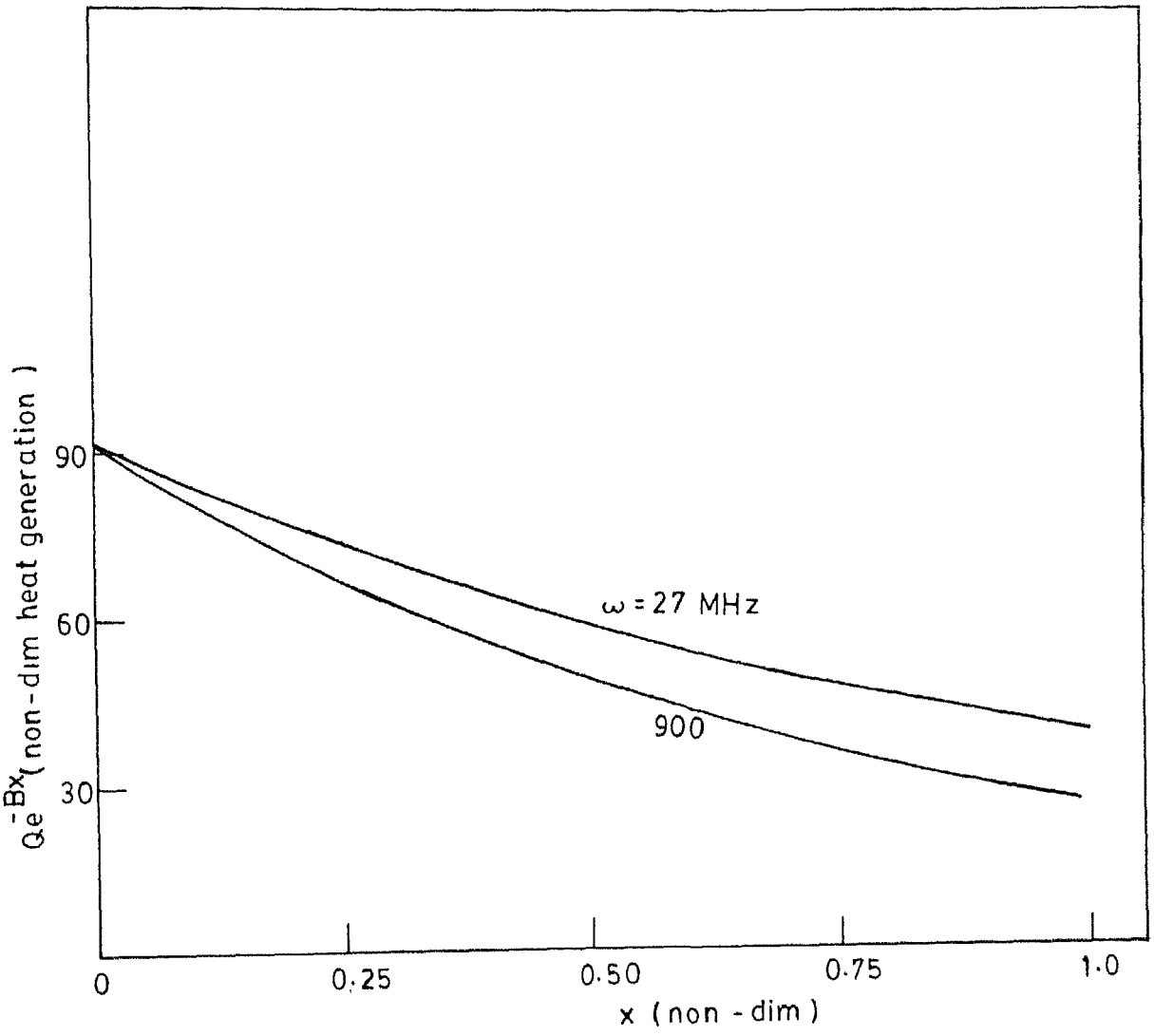

FIG. 4.7 b EFEECT OF FREQUENCY ON NON-DIM HEAT GENERATION ALONG THE DEPTH IN MUSCLE

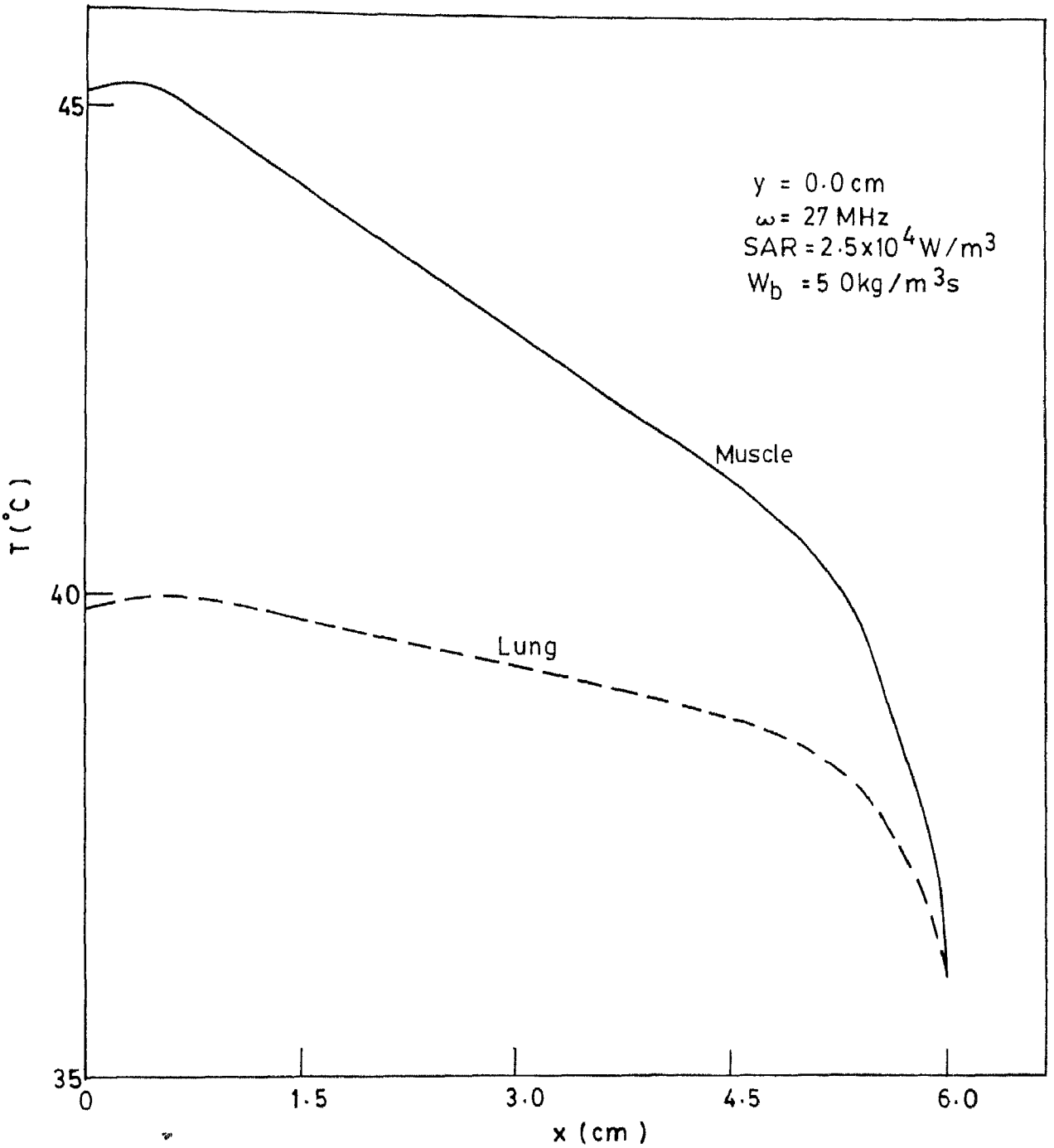

FIG. 4.8 A COMPARISON OF STEADY TEMPERATURE PROFILES FOR MUSCLE AND LUNG

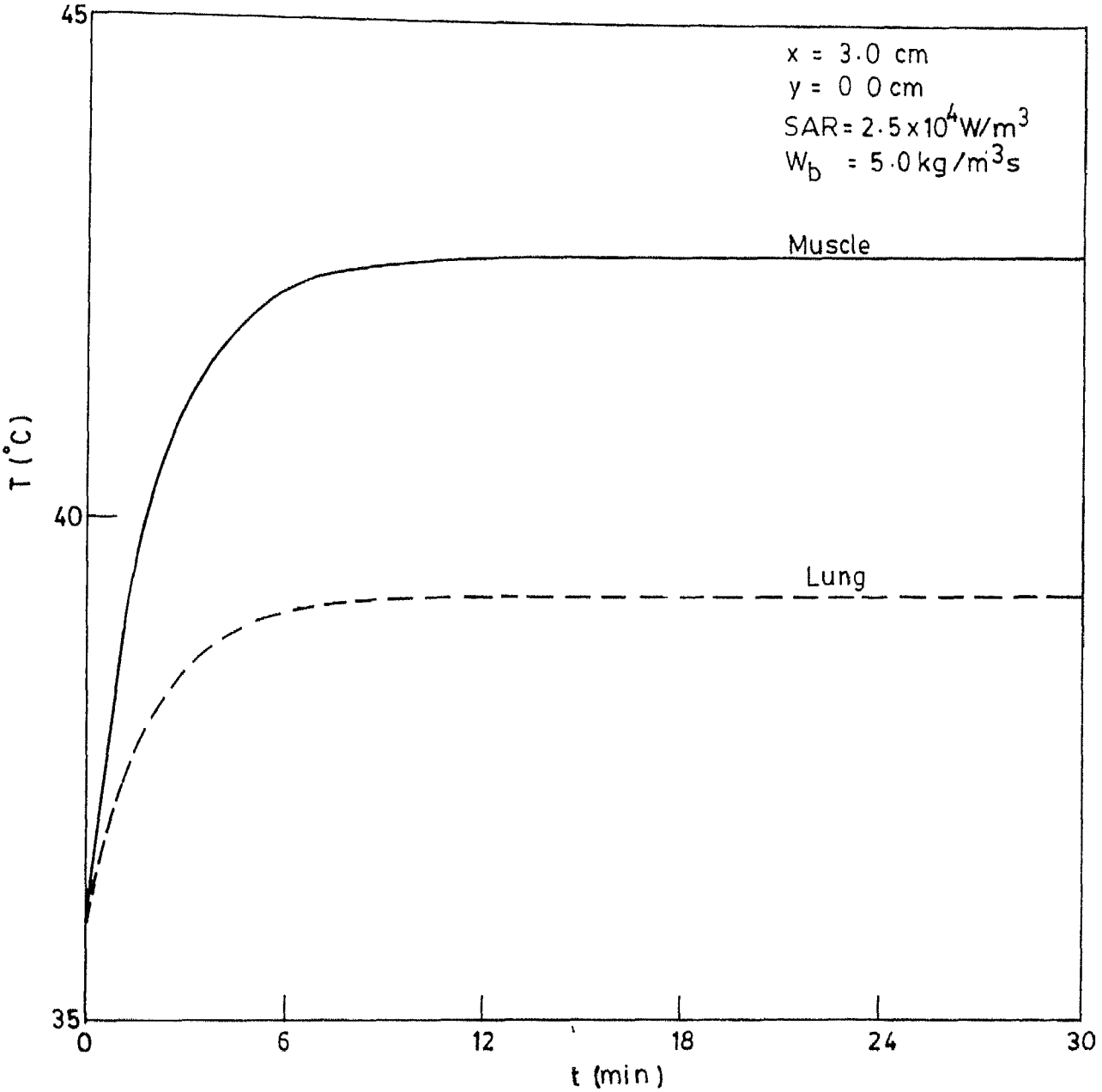

FIG. 4.9 A COMPARISON OF TRANSIENT TISSUE CENTRE TEMPERATURE FOR MUSCLE AND LUNG

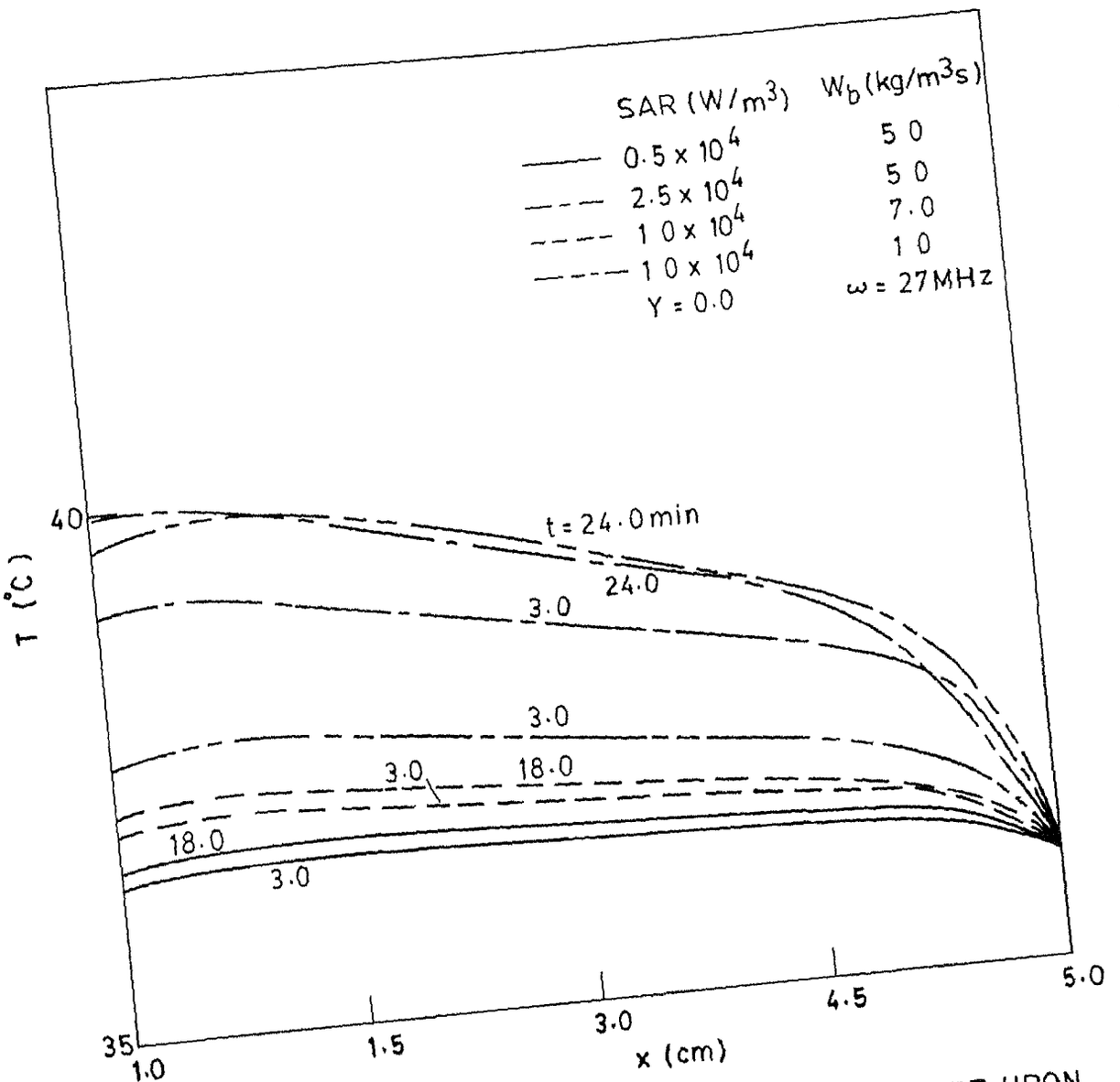

FIG. 4.10 EFFECT OF SAR AND BLOOD PERFUSION RATE UPON TRANSIENT TEMPERATURE DISTRIBUTION IN LUNG

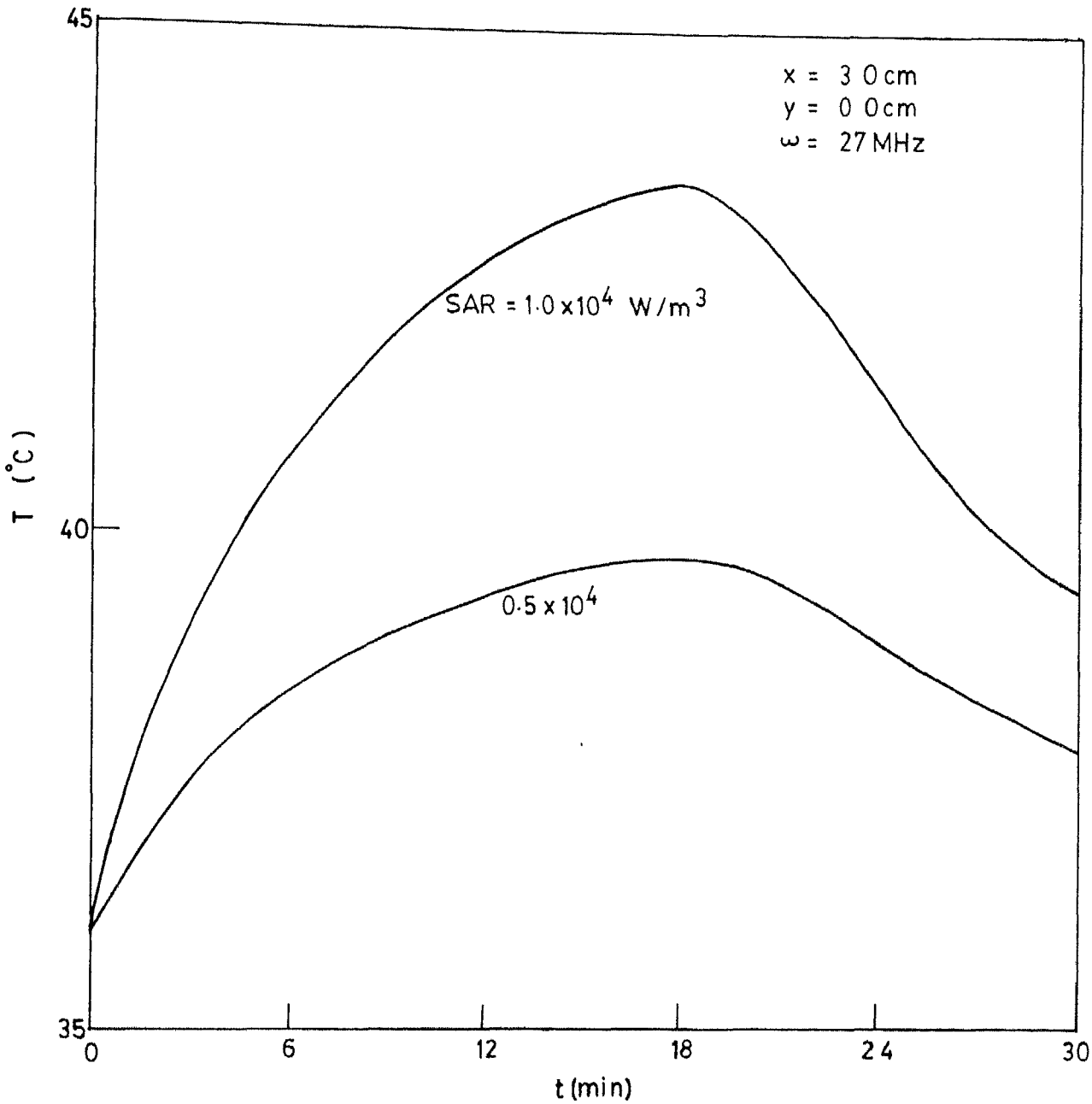

FIG. 4·11 MUSCLE CENTRE TEMPERATURE VARIATION WITH TIME FOR VARYING BLOOD PERFUSION RATE

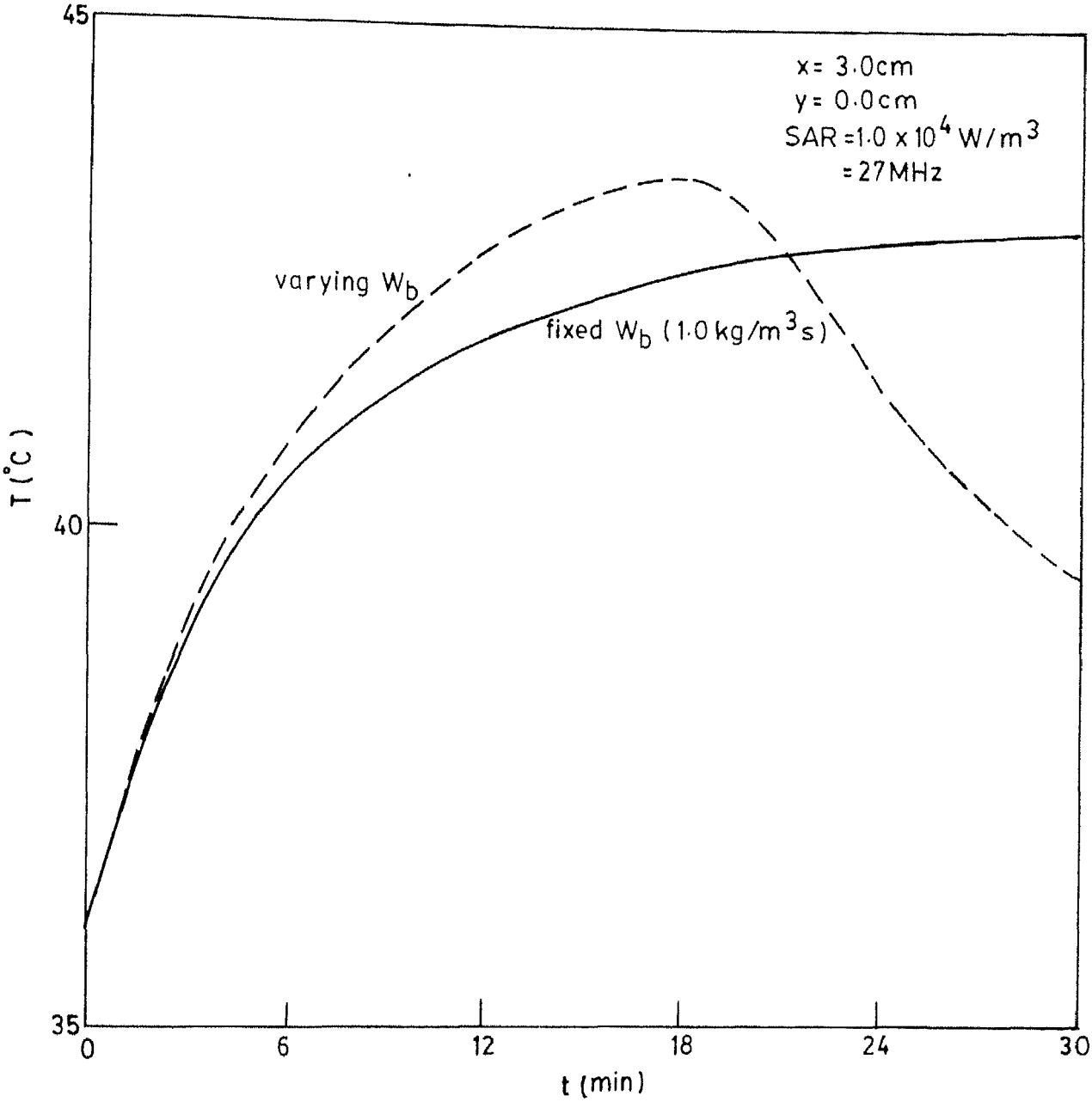

FIG. 4.12 A COMPARISON OF TRANSIENT MUSCLE CENTRE TEMPERATURE FOR FIXED AND VARYING BLOOD PERFUSION

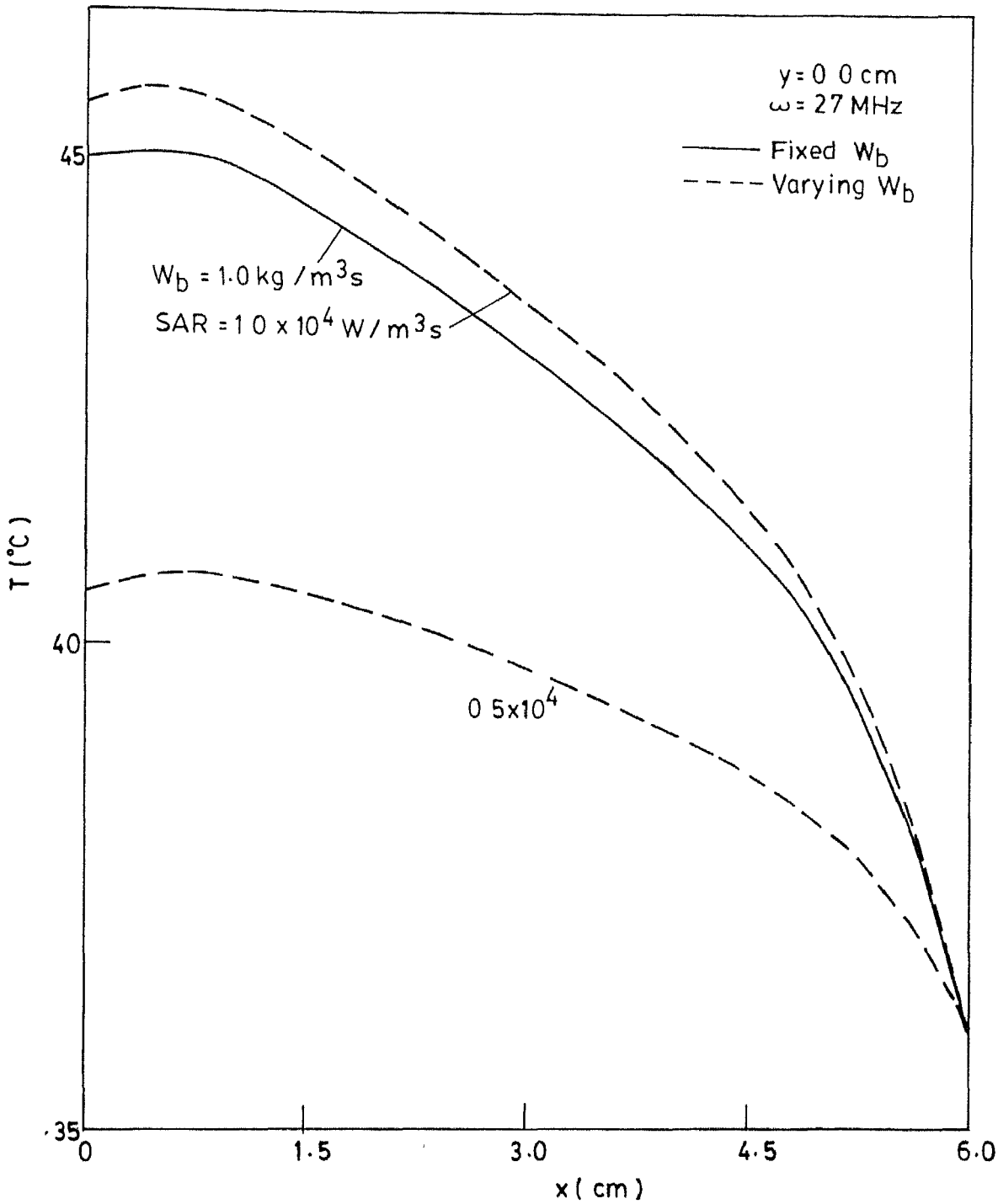

FIG. 4·13 A COMPARISON OF STEADY STATE TEMPERATURE PROFILES FOR FIXED AND VARYING BLOOD PERFUSION IN MUSCLE

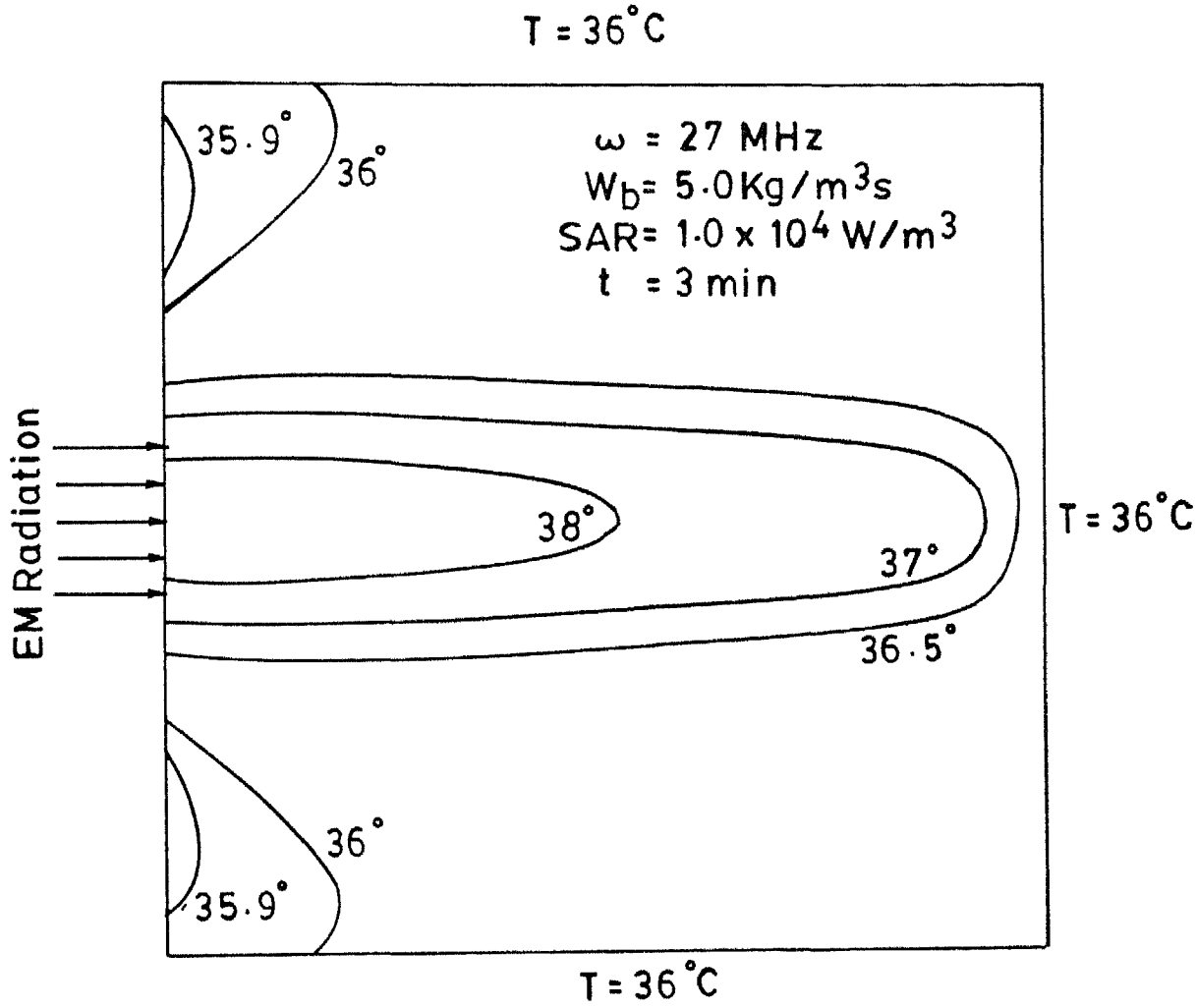

FIG. 4.14a ISOTHERM PATTERN IN MUSCLE FOR FIXED BLOOD PERFUSSION RATE

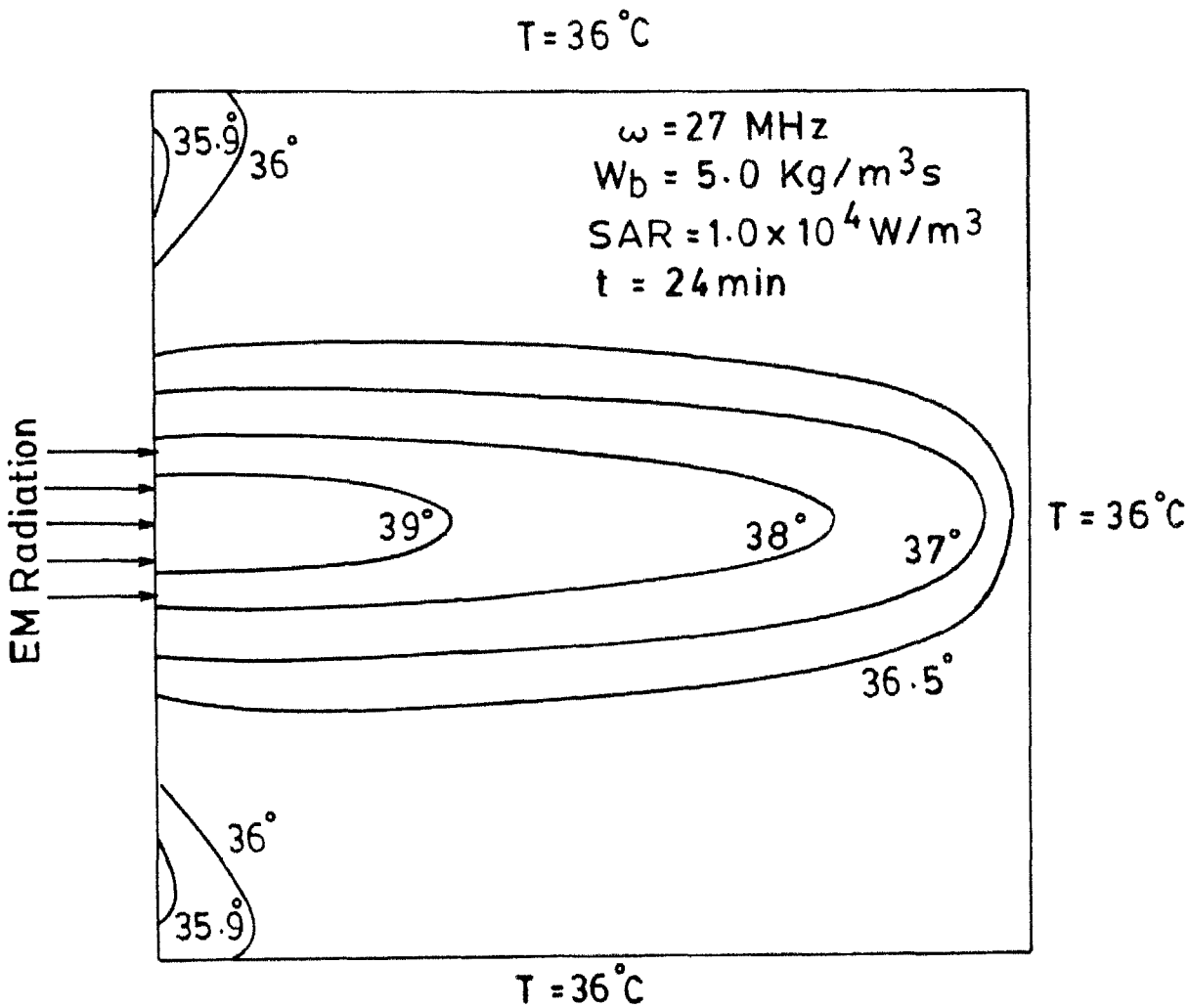

FIG. 4.14b ISOTHERM PATTERN IN MUSCLE FOR FIXED BLOOD PERFUSSION RATE

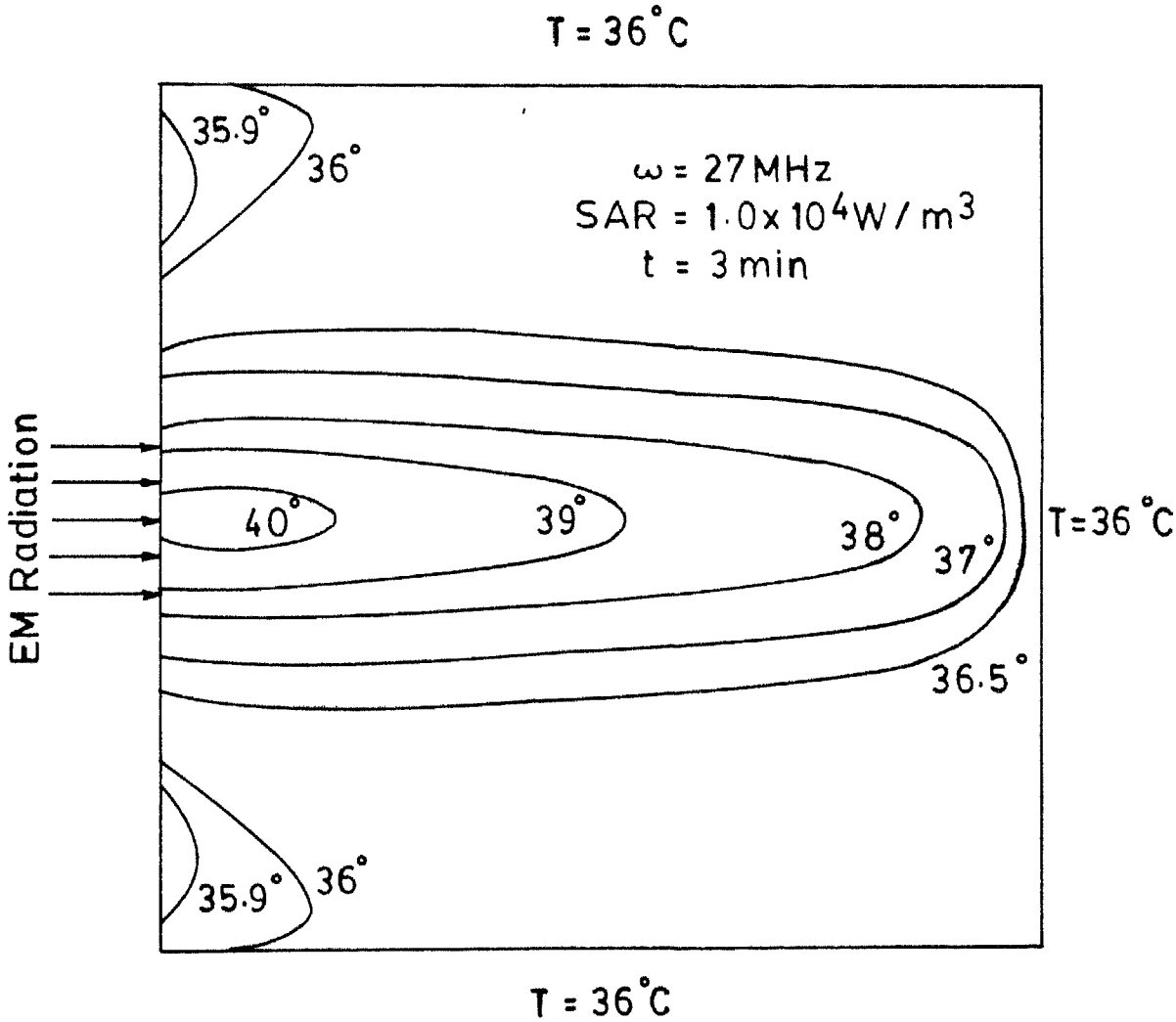

FIG. 4.14c ISOTHERM PATTERN IN MUSCLE FOR VARYING BLOOD PERFUSION RATE

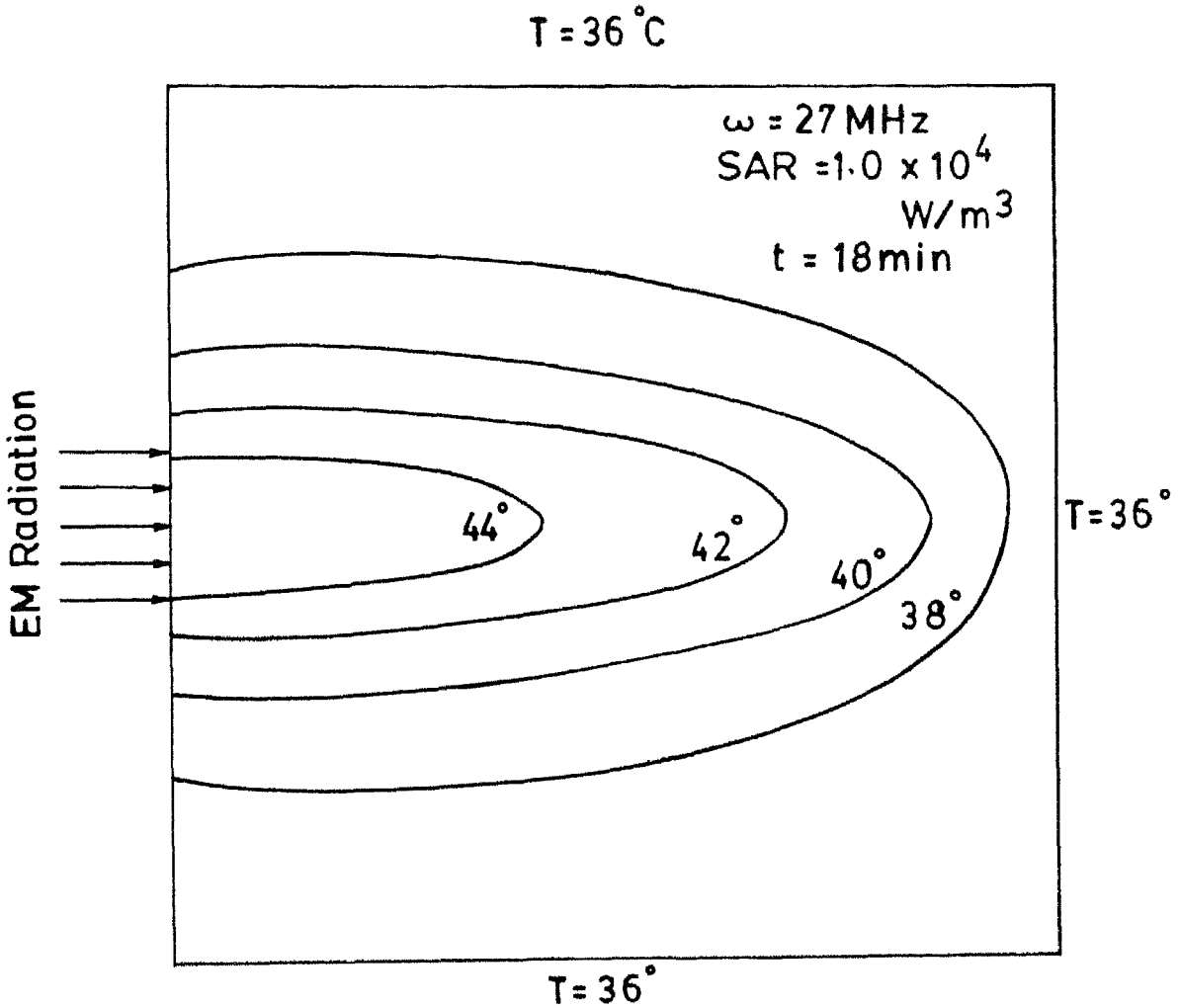

FIG. 4.14d ISOTHERM PATTERN IN MUSCLE FOR VARYING BLOOD PERFUSION RATE

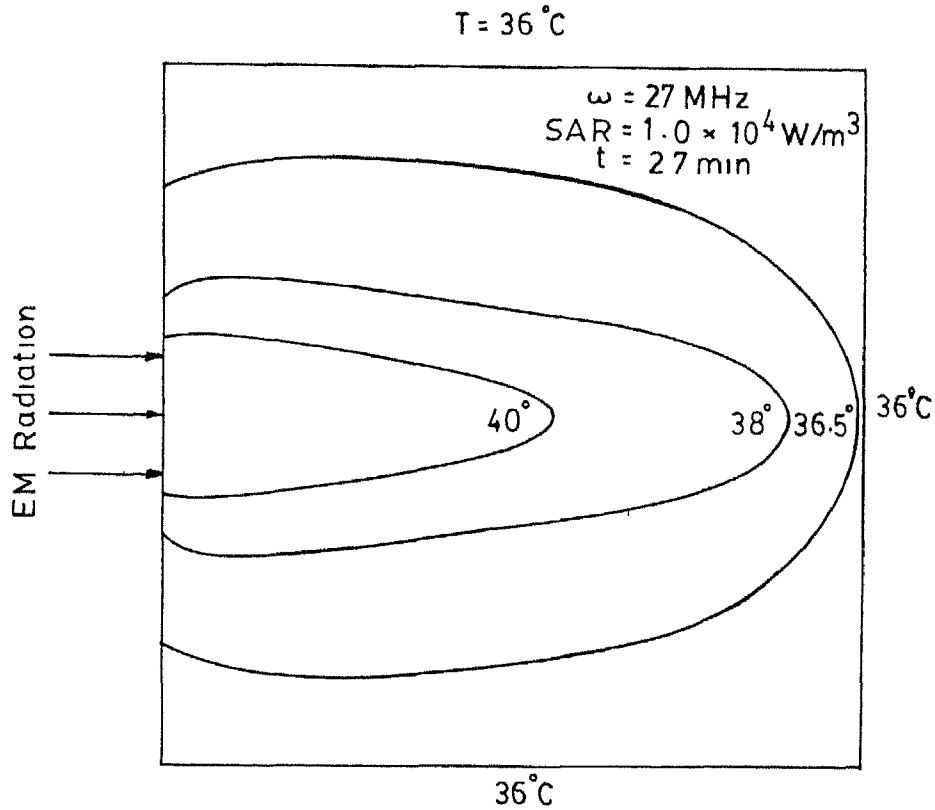

FIG 4.14e ISOTHERM PATTERN IN MUSCLE FOR VARYING BLOOD PERFUSION RATE

CHAPTER 5

CONCLUSIONS AND SUGGESTIONS

5.1 Conclusions

(1) Detailed numerical results have been obtained whose validity has been checked with an available analytical solution for a special case.

(2) The increase in temperature level is more sensitive to SAR than to blood perfusion rate.

(3) When blood perfusion rate varies automatically (as in a real tissue) the temperature has an overshoot and subsequent decrease to the final steady state value. This is due to the time lag associated with the increase in blood perfusion rate, as a response to the increase in tissue temperature.

(4) At lower frequencies, the volumetric rate of heat generation is higher compared to that at higher frequencies. Also, the decay of the heat generated with depth, is less steep for lower frequency levels. Therefore at low frequencies, the temperature level is higher and it decays more slowly with depth.

5.2 Suggestions

(1) The present problem can easily be extended to three dimensional or other complex geometries.

(2) The phenomenon of variable blood perfusion rate can be looked into more deeply.

(3) More complex situations, which considers the effect of (i) unidirectional and countercurrent blood vessels, (ii) microstructure of tissue, (iii) metabolic heat generation etc., can be focussed deeply for the present study.

REFERENCES

1. J.W. Baish, K.R. Foster, P.S. Ayyaswamy, 'Perfused Phantom Models of Microwave Irradiated Tissue', Journal of Biomechanical Engineering (ASME), Vol. 108, August 1986, p. 239.

2. J.W. Baish, P.S. Ayyaswamy, K.R. Foster, 'Small-scale Temperature Fluctuations in Perfused Tissue During Local Hyperthermia', Journal of Biomechanical Engineering (ASME), Vol. 108, August 1986, p. 246.

3. J.W. Baish, P.S. Ayyaswamy, K.R. Foster, 'Heat-Transport Mechanisms in Vascular Tissues: A Model Comparison', Journal of Biomechanical Engineering (ASME), Vol. 108, Nov. 1986, p. 324.

4. S. Weinbaum, L.M. Jiji, D.E. Lemons, 'Theory and Experiment for the Effect of Vascular Microstructure on Surface Tissue Heat Transfer - Part I : Anatomical Foundation and Model Conceptualization', Journal of Biomechanical Engineering (ASME), Vol. 106, Nov. 1984, p. 321.

5. L.M. Jiji, S. Weinbaum, D.E. Lemons, 'Theory and Experiment for the Effect of Vasculas Microstructure of Surface Tissue Heat Transfer - Part II: Model Formulation and Solution', Journal Biomechanical Engineering (ASME), Vol. 106, Nov. 1984, p. 331.

6. S. Weinbaum, L.M. Jiji, 'A New Simplified Bio-heat Equation for the Effect of Blood Flow on Local Average Tissue Temperature', Journal of Biomechanical Engineering (ASME), Vol. 107, May 1986, p. 131.

7. H. Arkin, K.R. Holmes, M.M. Chen, 'A Sensitivity Analysis of the Thermal Pulse Decay Method for Measurement of Local Tissue Conductivity and Blood Perfusion', Journal of Biomechanical Engineering (ASME), Vol. 108, Feb. 1986.

8. H. Arkin, K.R. Holmes, M.M. Chen, W.G. Bottje, 'Thermal Pulse Decay Method for Simultaneous Measurement of Local Thermal Conductivity and Blood Perfusion: A Theoretical Analysis', Journal of Bio-mechanical Engineering, Vol. 108, Aug. 1986, p. 208.

9. J.W. Valvano, J.T. Allen and H.F. Bowman, 'The Simultaneous Measurement of Thermal Conductivity, Thermal Diffusivity, and Perfusion in Small Volumes of Tissue', Journal of Biomechanical Engineering, Vol. 106, August 1984, p. 192.

10. K.M. Sekins, A.F. Emery, J.F. Lehmann, J.A.MacDougall, 'Determination of Perfusion Field during Local Hyperthermia with the Aid of Finite Element Thermal Models', Journal of Biomechanical Engineering, Vol. 104, Nov. 1982, p. 272.

11. K.R. Foster, P.S. Ayyaswamy, T. Sundararajan, K. Ramakrishna, 'Heat Transfer in Surface Cooled Objects Subject to Microwave Heating', IEE Transactions on Microwave Theory and Techniques, Vol. MTT-30, No.8, August 1980.

12. K.R. Diller, L.J. Hayes, 'A Finite Element Model of Burn Injury in Blood-Perfused Skin', Journal of Biomechanical Engineering, Vol. 105, August 1983, p. 300.

13. W.H. Newman, P.P. Lele, 'A Transient Heating Technique for the Measurement of Thermal Properties of Perfused Biological Tissue', Journal of Biomechanical Engineering, Vol. 107, August 1985, p. 219.

14. A.B. Elkowitz, A. Shitzer, R.C. Eberhart, 'Transient Temperature Profiles in Tissues with Non-uniform Blood Flow Distributions', Journal of Biomechanical Engineering, Vol. 104, August 1982, p. 202.

15. J.F. Deford, O.P. Gandhi, 'Calculation of Three-Dimensional Patterns for RF Hyperthemia', Workshop on Bio-electromagnetics, IEE Aug. 1 & 2, 1986, New Delhi.

16. J. Behari, 'Dielectric Dispersion and Mechanism of Microwave Interaction in Biological Media', Workshop on Bio-electromagnetics, IEE, August 1&2, 1986, New Delhi.

17. O.P. Gandhi, J.Y. Chen, A. Riazi, 'Currents Induced in a Human Being for Plane-wave Exposure Condition 0-50 MHz and for RF Scalers', Workshop on Bio-Electromagnetics, IEE, August 1&2, 1986, New Delhi.

18. R. Siegel, J.R. Howell, 'Thermal Radiation Heat Transfer'.

19. C. Taylor, T.G. Hughes, 'Finite Element Programming of the Navier-Stokes Equation'.

20. B.M. Irons, 'A Frontal Solution Program for Finite Element Analysis', Int. J. Num. Meth. in Engg., Vol. 2, 1970.

APPENDIX A

An analytical solution of the bio-heat transfer equation (2.28) is possible for steady state with boundary conditions as shown in Fig. (4.1). For such a situation, the problem becomes one-dimensional and the non-dimensional governing differential equation is:

$$\frac{d^2T}{dX^2} - WT + Q\, e^{-BX} = 0 \qquad (A.1)$$

To obtain the solution of equation (A.1), let us assume

$$T = T_h(X) + T_p(X) \qquad (A.2)$$

where $T_p(X)$ is the particular solution and $T_h(X)$ is the homogeneous solution, we shall assume $T_p(X)$ to be of the form:

$$T_p = \frac{Q}{W - B^2} \cdot e^{-BX} = C\, e^{-BX} \qquad (A.3)$$

where,

$$C = \frac{Q}{W - B^2}$$

Substituting for T_p in equation (A.1), we get,

$$\frac{d^2 T_h}{dX^2} - W T_h = 0 \qquad (A.4)$$

The general solution of equation (A.4) is given by:

$$T_h = A_1 \text{ Sinh } \sqrt{W}\, X + A_2 \text{ Cosh } \sqrt{W}\, X \qquad (A.5)$$

where A_1 and A_2 are constants to be determined from boundary conditions. The complete solution to equation (A.1) is, therefore:

$$T = A_1 \text{ Sinh} \sqrt{W}\, X + A_2 \text{ Cosh} \sqrt{W}\, X + C\, e^{-BX} \qquad (A.6)$$

Boundary Conditions:

i) $$\text{At } X = 0, \quad \frac{dT}{dX} = Bi[\, T - T_f^* \,] \qquad (A.7a)$$

This boundary condition gives rise to:

$$A_1 = \frac{Bi}{\sqrt{W}} \left[A_2 + C \left(1 + \frac{B}{Bi}\right) - T_f^* \right] \qquad (A.7b)$$

ii) $$\text{At } X = 1, \quad T = 0 \qquad (A.8a)$$

This boundary condition gives rise to:

$$A_1 \text{ Sinh } \sqrt{W} + A_2 \text{ Cosh } \sqrt{W} + C\, e^{-B} = 0 \qquad (A.8b)$$

Solving equation (A.7b) and equation (A.8b), A_1 and A_2 can be determined as:

$$A_2 = \frac{-Ce^{-B} + \sqrt{\frac{Bi}{W}} \left[T_f^* - C\left(1 + \frac{B}{Bi}\right)\right] \text{Sinh} \sqrt{W}}{\sqrt{\frac{Bi}{W}} \text{ Sinh} \sqrt{W} + \text{Cosh} \sqrt{W}} \qquad (A.9a)$$

$$A_1 = \frac{Bi}{\sqrt{W}} \left[A_2 - T_f^* + C\left(1 + \frac{B}{Bi}\right) \right] \qquad (A.9b)$$

Substituting for the constants A_1 and A_2 in equation (A.6) gives the complete solution for temperature.